THE JOURNAL OF BIOLOGICAL CHEMISTRY VOL. 290, NO. 41, pp. 24986–25011, October 9, 2015

Genome-wide Mechanosensitive MicroRNA (MechanomiR) Screen Uncovers Dysregulation of Their Regulatory Networks in the *mdm* Mouse Model of Muscular Dystrophy*

Received for publication, April 28, 2015, and in revised form, August 13, 2015 Published, JBC Papers in Press, August 13, 2015, DOI 10.1074/jbc.M115.659375

Junaith S. Mohamed[1], **Ameena Hajira, Michael A. Lopez, and Aladin M. Boriek**[2]

From the Pulmonary and Critical Care Section, Department of Medicine, Baylor College of Medicine, Houston, Texas 77030

Background: Dysregulation of mechanosensitive gene regulatory pathways is associated with muscular dystrophies.
Results: Genome-wide microRNA analyses revealed dysregulation of pathways controlled by let-7e-5p and miR-98–5p in dystrophic muscle.
Conclusion: Impaired mechanomiR-controlled pathways may contribute to muscular dystrophies.
Significance: MechanomiR-dependent pathways regulating extracellular matrix proteins and myogenesis are potential therapeutic targets for ameliorating muscle fibrosis and regeneration.

Muscular dystrophies (MDs) are a heterogeneous group of genetic and neuromuscular disorders, which result in severe loss of motor ability and skeletal muscle mass and function. Aberrant mechanotransduction and dysregulated-microRNA pathways are often associated with the progression of MD. Here, we hypothesized that dysregulation of mechanosensitive microRNAs (mechanomiRs) in dystrophic skeletal muscle plays a major role in the progression of MD. To test our hypothesis, we performed a genome-wide expression profile of anisotropically regulated mechanomiRs and bioinformatically analyzed their target gene networks. We assessed their functional roles in the advancement of MD using diaphragm muscles from *mdm* (MD with myositis) mice, an animal model of human tibial MD (titinopathy), and their wild-type littermates. We were able to show that *ex vivo* anisotropic mechanical stretch significantly alters the miRNA expression profile in diaphragm muscles from WT and *mdm* mice; as a result, some of the genes associated with MDs are dysregulated in *mdm* mice due to differential regulation of a distinct set of mechanomiRs. Interestingly, we found a contrasting expression pattern of the highly expressed let-7 family mechanomiRs, let-7e-5p and miR-98–5p, and their target genes associated with the extracellular matrix and TGF-β pathways, respectively, between WT and *mdm* mice. Gain- and loss-of-function analysis of let-7e-5p in myocytes isolated from the diaphragms of WT and *mdm* mice confirmed *Col1a1*, *Col1a2*, *Col3a1*, *Col24a1*, *Col27a1*, *Itga1*, *Itga4*, *Scd1*, and *Thbs1* as target genes of let-7e-5p. Furthermore, we found that miR-98 negatively regulates myoblast differentiation. Our study therefore introduces additional biological players in the regulation of skeletal muscle structure and myogenesis that may contribute to unexplained disorders of MD.

Skeletal muscle is a highly plastic tissue that has the ability to adapt to physiological and non-physiological conditions in response to mechanical stress. Unfortunately, this plasticity is completely absent in muscular dystrophies (MDs),[3] a heterogeneous group of genetic and neuromuscular disorders. MD causes severe loss of motor ability, skeletal muscle mass, strength, and function, mostly due to the loss of function of structural proteins such as dystrophin (Becker and Duchenne MDs) (1, 2) or due to the mutation of cytoskeletal genes such as *titin* (tibial distal MD and limb girdle MD) (3).

Mechanotransduction is a ubiquitous biophysical process by which cells sense their physical environment by translating physical forces and deformations into biochemical signals such as changes in intracellular calcium concentration and/or the activation of diverse signaling pathways (4–7). Such signaling pathways are essential for a wide range of cellular functions such as apoptosis, proliferation, differentiation, and migration, which are vital for organ development and cellular homeostasis. Defects in mechanotransduction are implicated in the development of many diseases, ranging from MDs, cardiomyopathies, and loss of hearing to cancer progression and metastasis (8). In Duchenne MD (DMD), the most common form of MD in children whose life expectancy extends only to the teens or early 20s, mutations in the dystrophin gene disrupt the force transmission between the cytoskeleton and the extracellular matrix (ECM) proteins resulting in progressive muscle degeneration (9). We have shown previously that disruption of cytoskeleton-ECM coupling due to loss of dystrophin causes aberrant activation of the MAPK extracellular signal-regulated kinase 1/2 (ERK1/2) signaling and increased expression of the inflammatory cytokines interleukin-1β and tumor necrosis factor-α in

* This work was supported in part by National Institutes of Health Grant HL-63134 from the NHLBI. This work was also supported by the National Science Foundation. The authors declare that they have no conflicts of interest with the contents of this article.
[1] Present address: Div. of Exercise Physiology, Dept. of Human Performance, Ctr. for Cardiovascular and Respiratory Sciences, West Virginia University School of Medicine, Morgantown, WV 26506.
[2] To whom correspondence should be addressed. Tel.: 713-798-6091; Fax: 713-798-2050; E-mail: boriek@bcm.edu.

[3] The abbreviations used are: MD, muscular dystrophy; DMD, Duchenne muscular dystrophy; ECM, extracellular matrix; miRNA, microRNA; myomiR, myogenic skeletal muscle-enriched microRNA; mechanomiR, mechanosensitive microRNA; TS, transverse stretch; LS, longitudinal stretch.

response to mechanical stretch in diaphragm muscle from *mdx* mouse, an animal model of DMD (5, 10). Furthermore, loss of dystrophin in the *mdx* mouse causes mechanical stress-induced rupture of the plasma membrane, which allows influx of extracellular calcium. This leads to abnormal muscle contraction and physical damage of the cytoskeleton, subsequently resulting in the loss of muscle cells (11). In addition to dystrophin, other cytoskeletal proteins also play a major role in mechanotransduction. For example, we have shown previously that loss of desmin in the desmin null mouse or mutation of the *titin* gene in *mdm* mouse (MD with myositis), an animal model of human tibial MD (titinopathy), causes disturbed cellular mechanics, including reduced force generation and altered (passive) cytoskeletal stiffness, which can decrease the relaxation dynamics of myocytes in the diaphragm (12, 13). Alteration in the mechanotransduction pathways in the *mdm* mouse, caused by a small in-frame deletion within the *titin* gene, results in an induction of aberrant signaling pathways (7) and impaired myogenic differentiation (14). Other studies from our laboratory have shown that the α7-integrin and sarcoglycan complex serve important mechanical functions in the diaphragm by contributing to passive compliance, viscoelasticity, and modulation of its muscle contractile properties (15, 16). Overall, these studies suggest the roles of cytoskeletal proteins in force transmission and mechanotransduction and their implication in MDs. Therefore, investigating the relative contributions of mechanotransduction to muscular dysfunction may have important clinical implications, because defects in mechanotransduction pathways could potentially be attenuated with genetic and/or pharmacological reagents. However, information on the genome-wide mechanosensitive gene regulatory networks is essentially lacking. Identification of changes in the global gene-regulatory network in response to normal and defective mechanotransduction could potentially lead to new paths to therapeutic approaches to MDs.

MicroRNAs (miRNAs) are the most abundant and well studied small noncoding RNAs, which act as "master switches" of the genome to regulate the expression of diverse proteins and orchestrate multiple cellular pathways (17). Changes in miRNA expression profiles are often associated with skeletal muscle diseases including MDs (Refs. 18–20 and references therein). Therefore miRNAs are not only used as diagnostic and prognostic markers, but they also may reveal deep insights into disease pathology. Several miRNAs are ubiquitously expressed, whereas some are tissue-specific and others are enriched in specific tissues. For example, miR-1, miR-133a, miR-133b, miR-206, miR-208, miR-208b, miR-486, and miR-499 are skeletal muscle-enriched miRNAs. These specific miRNAs play crucial roles in skeletal muscle functions in health and disease, and therefore they are called myomiRs (18, 21, 22). Using microarray technology, we pioneered the discovery of several mechanosensitive microRNAs (hereafter, we use the term mechanomiRs) in human airway smooth muscle cell. For example, we uncovered a novel mechanosensing role of miR-26a in regulating an airway smooth muscle phenotype (23). Subsequently, others have identified and demonstrated the role of individual mechanomiR in the pathogenicity of human diseases (24–31). Interestingly, we have shown previously that loss of desmin protein in mice alters the miRNA expression profile and induces airway smooth muscle cell hypertrophy as a consequence of miR-26a up-regulation (32), suggesting a potential key role for the cytoskeletal protein in regulating miRNAs. It is important to note however that information on the genome-wide expression profile of mechanomiRs and their target gene regulatory networks associated with human diseases, including MDs, is completely lacking.

Force transmission in skeletal muscles varies greatly with muscle fiber architecture (33). Whereas the *in vivo* skeletal muscles of either the hindlimb or forelimb are essentially mechanically loaded along the direction of the muscle fiber, the diaphragm muscle is mechanically loaded with trans-diaphragmatic pressure. Therefore, the diaphragm muscles are subjected to mechanical forces not only in the direction of the muscle fibers but also in a direction transverse to the fibers (33). The diaphragm, in particular, is the principal pressure-generating skeletal muscle that drives ventilation. Alteration of its mechanical properties could contribute to compromised respiratory muscle function. It is therefore important to determine how mechanotransduction is executed in the diaphragm muscle fibers in response to longitudinal and transverse directional forces. In agreement with this, we have shown previously the activation of two distinct signaling pathways, which are dependent on the direction of applied mechanical stretch in mouse diaphragm (4, 7). In particular, stretching the diaphragm along the muscle fibers up-regulates *Ankrd2* gene expression via the Akt/NF-κB pathway, whereas stretching of the diaphragm transverse to the muscle fibers up-regulates the same gene, *Aknrd2*, via the Ras/Raf-1/ERK-1/2/AP-1 pathway, strongly suggesting anisotropic regulation of gene expression in the diaphragm (7). Therefore, it was important to uncover potential genome-wide anisotropically regulated mechanomiRs and their target gene regulatory networks in the diaphragm muscle in response to directional mechanical stretches. To explore this, in the present study, we used *mdm* mice and their WT littermates. *Mdm* is an early-onset autosomal recessive disease caused by a complex rearrangement mutation in the mouse *titin* gene that leads to an in-frame 83-amino acid deletion in the N2A region of titin (34). The physiological importance of the titin N2A region is underscored by the severe disease it causes in the *mdm* mouse. It is important to recognize that the *mdm* mouse model exhibits a clinical phenotype similar to that of DMD. In particular, the *mdm* mouse has an early-onset, rapidly progressing, muscle-wasting disease that ends in premature death, likely due to respiratory insufficiency. In addition, the m-line and N2A *titin* mutations abolish one of many putative binding sites for calpain-3, a muscle-specific protease, and the loss of calpain-3 is linked to limb girdle MD 2A (35). Histopathology of the tibial muscle in human MD has been reported to be similar to that in skeletal muscles of the *mdm* mouse (3). Therefore, there is a strong rationale to utilize *mdm* mice to study the molecular mechanisms that cause the progression and severity of MDs in human.

In the present study, using miRNA microarray followed by bioinformatics analyses, we identified differentially regulated mechanomiRs and their predicted target genes and associated biological pathways. We found that mechanomiRs from the

let-7 family members, especially let-7e-5p and miR-98–5p, were highly dysregulated in the diaphragm of the *mdm* mouse. Using an *in vitro* validation method, we identified *Col1a1*, *Col1a2*, *Col3a1*, *Col24a1*, *Col27a1*, *Itga1*, *Itga4*, *Scd1*, and *Thbs1* as target genes of let-7e-5p. Furthermore, we identified a role for miR-98–5p as a negative regulator of myoblast differentiation. We also found stretch-induced up-regulation of the TGF-β1 signaling pathway in diaphragm muscle from the *mdm* mouse. Finally, we were able to revoke the stretch-induced up-regulation of ECM proteins by restoring let-7e-5p and the stretch-induced inhibition of myoblast differentiation by reinstating miR-98–5p in primary myoblasts. Overall, we uncovered a role for mechanomiR in skeletal muscle function and propose that dysregulation of mechanomiRs may be associated with the development of human skeletal muscle diseases including MD.

Experimental Procedures

Mice and ex Vivo Mechanical Loading of Diaphragms—The C57BL/6JWT and B6.B6C3Fe-Ttn*mdm* J/Cx strain mice were obtained from The Jackson Laboratory (Bar Harbor, ME). Mice were maintained in accordance with the National Institutes of Health Guide for the Care and Use of Laboratory Animals and the approved animal protocols of the Institutional Animal Care and Use Committee of Baylor College of Medicine. In all experiments, we used diaphragms from 2-week-old *mdm* mice and their WT littermates. Each experiment was repeated at least three times in three different mice. Tissue preparation and *ex vivo* stretch were performed as described earlier (4, 7, 13). Briefly, mechanical stretch was applied to the entire costal muscles of the left hemidiaphragm (the right hemidiaphragm muscle was treated as an unstretched control with an environment similar to that of the left hemidiaphragm) by passively stretching the muscle in the longitudinal or transverse direction to the muscle fibers with a passive tension of ~0.4 newton/cm. This application was equivalent to a passive stress of ~11 newtons/cm^2. A mechanical stretch of nearly 50% from the unstressed state was achieved in the normal diaphragm muscle. It is important to recognize that the unstressed length or the length of the excised muscle is the shortest muscle length and is equivalent to diaphragm muscle length at a lung volume of total lung capacity. The optimal length is about 125% of this unstressed length. Therefore, our stretch of 50% placed the diaphragm at a length equivalent to 120% of optimal muscle length. In each of these two stretch protocols, the diaphragm muscle was held in the stretched state for 15 min and then immediately processed for RNA or cell lysate extraction.

MicroRNA Microarray Analysis—Total RNA samples were isolated from unstretched or stretched hemidiaphragms by TRIzol reagent according to the manufacturer's protocol (Invitrogen). Ten micrograms of total RNA was size-fractionated with a YM-100 Microcon centrifugal filter (Millipore, Billerica, MA) and then used for miRNA expression analysis with a miRNA microarray using their proprietary μParaFlo microfluidic chip containing 700 mouse standard mature miRNA probes (Sanger miRBase 14.0). The fold difference values of altered mechanomiRs were converted into $\log_2$ scale.

TABLE 1
Sequences of mouse primers used in real-time PCR

Gene	Primer sequence 5'→ 3'	Ref. Seq ID	cDNA Size
Col1a1	F: TAGGCCATTGTGTATGCAGC	NM_007742	110
	R: ACATGTTCAGCTTTGTGGACC		
Col1a2	F: AGCAGGTCCTTGGAAACCTT	NM_007743	101
	R: AAGGAGTTTCATCTGGCCCT		
Col3a1	F: TAGGACTGACCAAGGTGGCT	NM_009930	98
	R: GGAACCTGGTTTCTTCTCACC		
Col24a1	F: TGCCTATATTGAGTCACCTCTCG	NM_027770	130
	R: TCTGTTGTTATTCCGAATGCTGA		
Col27a1	F: AGTCCTGGGTCCCCTTTCT	NM_025685	124
	R: CTGGGCTTCCAGGATTACCT		
Itga1	F: AGGCCGAATTTGGATACAGTG	NM_001081053	118
	R: GAGCAACGATAAACATCCCCTC		
Itga4	F: AATGCCTCAGTGGTCAATCC	NM_010576	89
	R: CTACCCAGCTGGAGCTGTTC		
Scd1	F: ACTGTGGAGACGTGTTCTGGA	NM_177618	191
	R: ACGGGTGTCTGGTAGACCTC		
Thbs1	F: CCTGCCAGGGAAGCAACAA	NM_011580	115
	R: ACAGTCTATGTAGAGTTGAGCCC		
Drosha	F: ATGCAAGGCAATACGTGTCAT	NM_026799	110
	R: TTTTGGGGTCTGAAAGCTGGT		
Dicer1	F: GGTCCTTTCTTTGGACTGCCA	NM_148948	149
	R: GCGATGAACGTCTTCCCTGA		
Exportin5	F: TGTGCGAGGAGCTAGTGAAAG	NM_028198	167
	R: TCTGACGATGGCAATTTGTGTT		
DGCR8	F: GCAGGAGAAGCGATGATGGAG	NM_033324	170
	R: CCGTAGAAGTTGAATGGGTCG		
Ago1	F: CAGCAGGTGTTTCAGGCAC	NM_153403	143
	R: GGACACTTATCCGGCTTGATG		
Ago2	F: GGCGTTACACGATGCACTTTC	NM_153178	158
	CACCCAGAGGGTTGGAACAG		
Ago3	F: GGGTATGGCACTATGGGCAAA	NM_153402	122
	R: ACTCTTCGAGGACACTTGTCT		
Ago5	F: GGTCCTGGTCCTTGGAACAG	XR_106050	134
	R: GCAGGGAGGTGGAAACTCTC		

Gene Functional Analysis—To identify the predicted-biological pathways regulated by mechanomiRs (≥2.0-fold), we used the DIANA miRPath v2.0 Web-based computational tool with a threshold p value of 0.05 and a MicroT threshold value of 0.8 (36). MechanomiRs and their predicted targets were identified using the miRWalk Web-based computational tool, which provides miRNA targets from at least eight established miRNA prediction programs (37).

Real-time PCR Expression Analysis—For miRNA expression analysis, we used a TaqMan advanced miRNA cDNA synthesis kit and TaqMan advanced miRNA assays to quantify mature miRNAs according to the manufacturer's protocol (Applied Biosystems, Grand Island, NY). mRNA expression levels were quantified by real-time analysis as mentioned earlier (23). Primer sequences are given in Table 1. All PCR products were verified on an agarose gel stained with ethidium bromide to discriminate between the correct amplification products and the potential primer dimers.

Solution Hybridization Detection Analysis—The expression levels of mature miRNAs were measured by a solution hybridization detection method using mirVana miRNA and BrightStar BioDetect kits (Ambion) as described previously (23).

Immunoblots—Immunoblots were performed as documented earlier (14). Col1a1, Col1a2, Col3a1, Col24a1, Col27a1, Itga1, Itga4, Scd1, Thbs1, and GAPDH antibodies were purchased from Santa Cruz Biotechnology, Inc., Dallas, TX. TGF-

TABLE 2

Differentially regulated mechanomiRs in diaphragm from WT mouse

Bold indicates differentially regulated mechanomiRs by longitudinal and transverse stretches. Underlines indicate differentially regulated mechanomiRs at signal intensities > 10,000.

Longitudinal stretch					
No	MechanomiRs	p-value	Stretch	No stretch	Log_2
1	miR-30e	1.39E-05	1080	278	1.96
2	miR-451	8.94E-06	794	226	1.81
3	miR-22	3.75E-05	1525	435	1.81
4	miR-30c	2.33E-05	2851	901	1.66
5	miR-30b	3.46E-05	1413	460	1.62
6	miR-125b-5p	3.08E-05	5642	2097	1.43
7	miR-30a	8.04E-05	2200	848	1.38
8	miR-322	3.82E-04	1054	412	1.36
9	miR-29a	2.86E-06	1302	536	1.28
10	**miR-126-3p**	8.17E-05	16197	6882	1.23
11	**miR-125a-5p**	7.69E-03	1749	786	1.15
12	miR-195	1.03E-03	1066	494	1.11
13	**miR-133b**	8.56E-06	9283	4410	1.07
14	miR-30d	1.34E-03	1674	802	1.06
15	**miR-27a**	4.40E-04	1765	853	1.05
16	**miR-133a**	4.44E-05	10374	5169	1.01
17	**miR-23a**	7.01E-03	11202	5589	1.00
18	**miR-16**	4.02E-03	2931	1503	0.96
19	**miR-690**	3.18E-03	2733	1429	0.94
20	**miR-27b**	9.41E-03	2134	1133	0.91
21	**miR-382**	2.73E-06	379	1806	-2.25
22	**miR-379**	6.85E-07	806	2986	-1.89
23	miR-21	9.10E-06	591	1907	-1.69
24	**miR-541**	1.00E-04	370	1170	-1.66
25	**miR-206**	1.38E-05	8428	25014	-1.57
26	**miR-127**	2.50E-05	1818	4430	-1.29
27	miR-214	2.00E-03	398	974	-1.29
28	let-7g	3.39E-04	2025	4685	-1.21
29	**miR-26a**	4.56E-04	9274	20475	-1.14
30	miR-487b	4.09E-03	401	885	-1.14
31	miR-25	3.31E-04	393	861	-1.13
32	miR-299*	1.02E-04	772	1662	-1.11
33	**miR-26b**	2.24E-03	1168	2478	-1.09
34	miR-709	2.69E-05	6148	12538	-1.03
35	**miR-199a-3p**	5.70E-03	1176	2262	-0.94
36	**miR-24**	6.02E-03	1940	3469	-0.84

TABLE 2—*continued*

Transverse stretch					
No	MechanomiRs	p-value	Stretch	No stretch	Log_2
1	miR-763	1.42E-04	677	59	3.52
2	let-7e	1.24E-07	6397	661	3.27
3	miR-98	3.54E-07	816	123	2.73
4	**miR-382**	1.62E-05	3987	1129	1.82
5	let-7b	1.54E-04	11197	3309	1.76
6	let-7d	9.23E-05	12930	3963	1.71
7	let-7c	1.53E-04	14814	4871	1.60
8	miR-705	1.56E-05	882	293	1.59
9	let-7a	5.10E-04	16531	5638	1.55
10	let-7f	1.55E-04	12958	4480	1.53
11	**miR-206**	5.08E-04	43613	15634	1.48
12	**miR-125a-5p**	2.50E-03	1902	786	1.28
13	miR-26b	1.40E-03	3611	1549	1.22
14	**miR-690**	2.35E-03	2931	1429	1.0 -
15	miR-411	5.18E-03	213	854	2.00
16	**miR-127**	3.90E-06	1253	4430	-1.82
17	**miR-26a**	1.88E-06	5829	20475	-1.81
18	**miR-199a-3p**	1.80E-04	649	2262	-1.80
19	miR-143	1.00E-03	467	1603	-1.78
20	**miR-133a**	8.77E-08	2433	8270	-1.77
21	miR-378	1.69E-03	805	2573	-1.68
22	**miR-133b**	8.86E-06	2231	7056	-1.66
23	**miR-23a**	1.16E-05	2930	8942	-1.61
24	miR-23b	1.88E-05	3179	9509	-1.58
25	**miR-27b**	1.63E-04	649	1813	-1.48
26	**miR-126-3p**	1.48E-05	4016	11011	-1.46
27	**miR-379**	2.85E-03	1136	2986	-1.39
28	**miR-27a**	1.20E-03	527	1365	-1.37
29	**miR-541**	4.35E-03	458	1170	-1.35
30	**miR-24**	7.36E-05	1399	3469	-1.31
31	miR-434-3p	1.61E-03	746	1853	-1.31
32	**miR-16**	4.98E-03	1111	2405	-1.11
33	miR-1	3.21E-03	29319	59747	-1.03

β1, SMAD, and pSMAD antibodies were purchased from Cell Signaling, Danvers, MA.

Primary Myoblast Isolation and in Vitro Experiments—Primary myoblasts from the diaphragm muscles of WT and *mdm* mice were isolated and cultured as described previously (14).

Transfection—Transfection of myocytes was performed as described previously (38), except 2.5 μg of expression vector bearing mmu-let-7e-5p or mmu-miR-98 –5p precursor, 400 ng of mmu-let-7e-5p or mmu-miR-98 –5p miRCURY LNA knockdown probe (antagomir), or scrambled probe (Exiqon Inc., Woburn, MA) was used.

Statistical Analysis—The results of our experiments are expressed as means ± S.E. Comparisons among different groups were performed by one-way analysis of variance followed by a Bonferroni test. A p value of <0.05 was considered statistically significant. Each experiment was repeated at least three times in three different mice.

Results

Identification of Genome-wide Anisotropically Regulated MechanomiRs in Diaphragm from WT Mouse—To identify the genome-wide expression of anisotropically regulated mechanomiRs in nondystrophic diaphragm, we performed miRNA microarray analyses using total RNA isolated from either longitudinally stretched or transversely stretched diaphragm from WT mouse. To eradicate false positives and identify miRNAs that had the highest chance of being mechanomiRs, we focused on those miRNAs with potential biological significance (signal

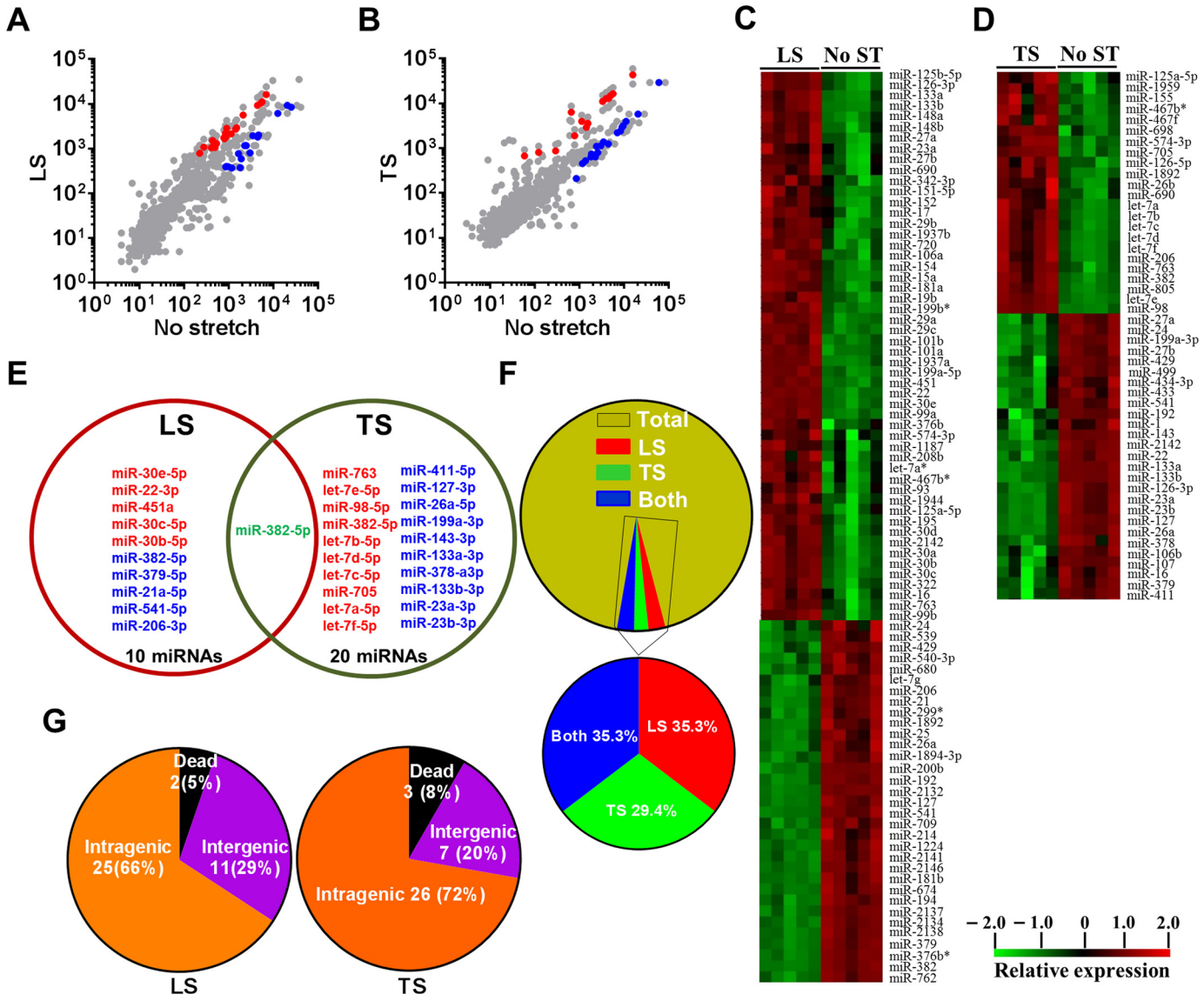

FIGURE 1. **Genome-wide expression profile of mechanomiRs in diaphragm from WT mouse.** Total RNA was isolated from either longitudinally or transversely stretched hemidiaphragm from WT mouse and used in miRNA microarray analyses to determine differentially regulated mechanomiRs. *A* and *B*, the scatter plot shows $\log_{10}$-transformed signal intensities for each probe labeled with Cy3 for unstretched (control) and Cy5 for LS (*A*) or TS (*B*) diaphragm. Each *dot* represents one miRNA probe. *C* and *D*, data on the heat map show differentially expressed mechanomiRs in diaphragm in response to LS (*C*) or TS (*D*). *E*, Venn diagram shows up (*red*)- and down (*blue*)-regulated mechanomiRs (>1.5-fold) after corresponding stretch. *F*, percentage of differentially expressed mechanomiRs to the total number of miRNAs in the array. *G*, percentage of differentially expressed mechanomiRs based on their genomic location.

intensity levels > 500) (39). Nearly 7.3% of an array of 700 miRNAs expressed a signal intensity > 500. MechanomiRs that were expressed with the highest signal intensity (>10,000) represented only 1.4% of the 700 analyzed miRNAs. Some of the highly expressed mechanomiRs in diaphragms from WT mice were myomiRs (*i.e.* miR-1, miR-133a, and miR-206), with miR-1 being the most highly expressed mechanomiR (59,747) followed by miR-206 (43,613) and miR-133a (10,374). Non-myomiRs such as miR-26a (20,475) and let-7 family members (>10,000) also displayed high signal intensities (Table 2). Of the 700 miRNA probes examined in the stretched or unstretched diaphragm muscle, the array uncovered the induction of 51 differentially regulated mechanomiRs (18 mechanomiRs were identified in response to only longitudinal stretch (LS), 15 mechanomiRs were identified in response to only transverse stretch (TS), and 18 mechanomiRs were identified in response to either LS or TS) (Fig. 1, *A*–*D*, and Table 2). Only 29 mechanomiRs, however, were differentially expressed at >1.5-fold (Table 3 and Fig. 1*E*) (nine mechanomiRs were identified in response to only LS, 19 mechanomiRs were identified in response to only TS, and a single mechanomiR was identified in response to either LS or TS). Of 29 mechanomiRs, LS and TS differentially regulated 10 (five up-regulated and five down-regulated) and 20 (10 up-regulated and 10 down-regulated) mechanomiRs, respectively, based on a p value of 0.01. By comparison, LS and TS altered 2.6 and 2.1% of the mechanomiRs (LS 35.3% and TS 29.4% of 51), respectively, among the total miRNAs in the array (Fig. 2*F*). Interestingly, both LS and TS altered 18 mechanomiRs (2.6%, which is 35.3% of 51) either in a similar manner or in an opposite manner (Table 2). For example, whereas LS and TS either up- or down-regulated miR-125a, miR-127, miR-199a, miR-24, miR-26a, miR-26b, miR-379,

TABLE 3

Differentially regulated mechanomiRs (>1.5-fold) in diaphragm from WT mouse

Bold indicates differentially regulated mechanomiRs by longitudinal and transverse stretches. Underlines indicate differentially regulated mechanomiRs at signal intensities > 10,000.

Longitudinal stretch						Transverse stretch					
No	**MechanomiRs**	**p-value**	**Mean**	**Mean**	**Log_2**	**No**	**MechanomiRs**	**p-value**	**Mean**	**Mean**	**Log_2**
1	miR-30e	1.39E-05	1080	278	1.96	5	let-7b	1.54E-04	11197	3309	1.76
2	miR-451	8.94E-06	794	226	1.81	6	let-7d	9.23E-05	12930	3963	1.71
3	miR-22	3.75E-05	1525	435	1.81	7	let-7c	1.53E-04	14814	4871	1.60
4	miR-30c	2.33E-05	2851	901	1.66	8	miR-705	1.56E-05	882	293	1.59
5	miR-30b	3.46E-05	1413	460	1.62	9	let-7a	5.10E-04	16531	5638	1.55
6	**miR-382**	2.73E-06	379	1806	-2.25	10	let-7f	1.55E-04	12958	4480	1.53
7	miR-379	6.85E-07	806	2986	-1.89	11	miR-411	5.18E-03	213	854	-2.00
8	miR-21	9.10E-06	591	1907	-1.69	12	miR-127	3.90E-06	1253	4430	-1.82
9	miR-541	1.00E-04	370	1170	-1.66	13	miR-26a	1.88E-06	5829	20475	-1.81
10	miR-206	1.38E-05	8428	25014	-1.57	14	miR-199a-3p	1.80E-04	649	2262	-1.80
Transverse stretch						15	miR-143	1.00E-03	467	1603	-1.78
1	miR-763	1.42E-04	677	59	3.52	16	miR-133a	8.77E-08	2433	8270	-1.77
2	let-7e	1.24E-07	6397	661	3.27	17	miR-378	1.69E-03	805	2573	-1.68
3	miR-98	3.54E-07	816	123	2.73	18	miR-133b	8.86E-06	2231	7056	-1.66
4	**miR-382**	1.62E-05	3987	1129	1.82	19	miR-23a	1.16E-05	2930	8942	-1.61
						20	miR-23b	1.88E-05	3179	9509	-1.58

miR-541, and miR-690, both directional stretches oppositely regulated miR-126, miR-133a, miR-133b, miR-16, miR-206, miR-23a, miR-27a, miR-27b, and miR-382. Of note, some of the differentially regulated mechanomiRs are the previously identified mechanomiRs such as miR-23b, miR-25, miR-30b, miR-126, miR-143, miR-145a, miR-214, and miR-21a in non-skeletal muscle tissues (28). Taken together, using miRNA array, we identified new sets of mechanomiRs from WT mouse diaphragm; the regulation of some of these mechanomiRs is dependent on the direction of stretch. We also identified a few mechanomiRs that are independent of the direction of applied stretch. With regard to highly regulated mechanomiRs (>1.5-fold), compared with LS, TS induced a higher number of mechanomiRs that are entirely different from the mechanomiRs induced by LS (except for miR-382).

Next, we grouped the mechanomiRs based on their genomic locations. We found that 25 (69.4%) and 26 (78.7%) mechanomiRs induced by LS and TS, respectively, were intragenic miRNAs, which are the highest number of mechanomiRs in the present study (Fig. 1*G*). On the other hand, 11 (15.9%) and seven (10.1%) mechanomiRs induced by LS and TS, respectively, were intergenic miRNAs, suggesting global regulation of mechanomiRs. However, a small number of mechanomiRs induced by LS (miR-2132 and miR-2142) or TS (miR-2142, miR-1224 and miR-805) were not included due to their prediction as "dead" miRNAs according to miRBase.

In addition, a significant number of mechanomiRs were derived from close genomic loci (<10 kb), encoded by bi- or polycistronic transcriptional units, which generate multiple miRNAs called miRNA clusters. Interestingly, these miRNA clusters have two different modes of transcription, yet their coordinated regulation during stretch indicated that they shared common regulatory features. In the present study, we found transcription of 40 mechanomiRs as clusters. LS induced the transcription of six clusters, which contained 16 mechanomiRs, whereas TS induced the transcription of 10 clusters, which contained 24 mechanomiRs (Table 4). Interestingly, some of the clusters of mechanomiRs were similar for LS and TS, suggesting that these clusters of mechanomiRs may have similar and/or coordinated biological functions.

Several differentially regulated mechanomiRs also fell into the same miRNA family. For example, LS and TS induced 17 and 19 mechanomiRs, respectively, which fell into 14 families. Interestingly, whereas LS and TS together induced the miR-26, miR-27, and miR-133 families, mechanomiRs belonging to the miR-10, miR-15, miR-30, and miR-154 families were induced only by LS, and let-7, miR-1, miR-23 and miR-379 were induced only by TS (Table 5). Because members within the same miRNA family share 5′-seed sequences, which are highly conserved 7- or 8-mer sequences within miRNAs (*e.g.* let-7 family), the identification of mechanomiRs in the same family may have target specificity and similar and/or coordinated biological functions. These findings suggest that the alteration in the mechanomiR expression profile occurred in a regulated manner.

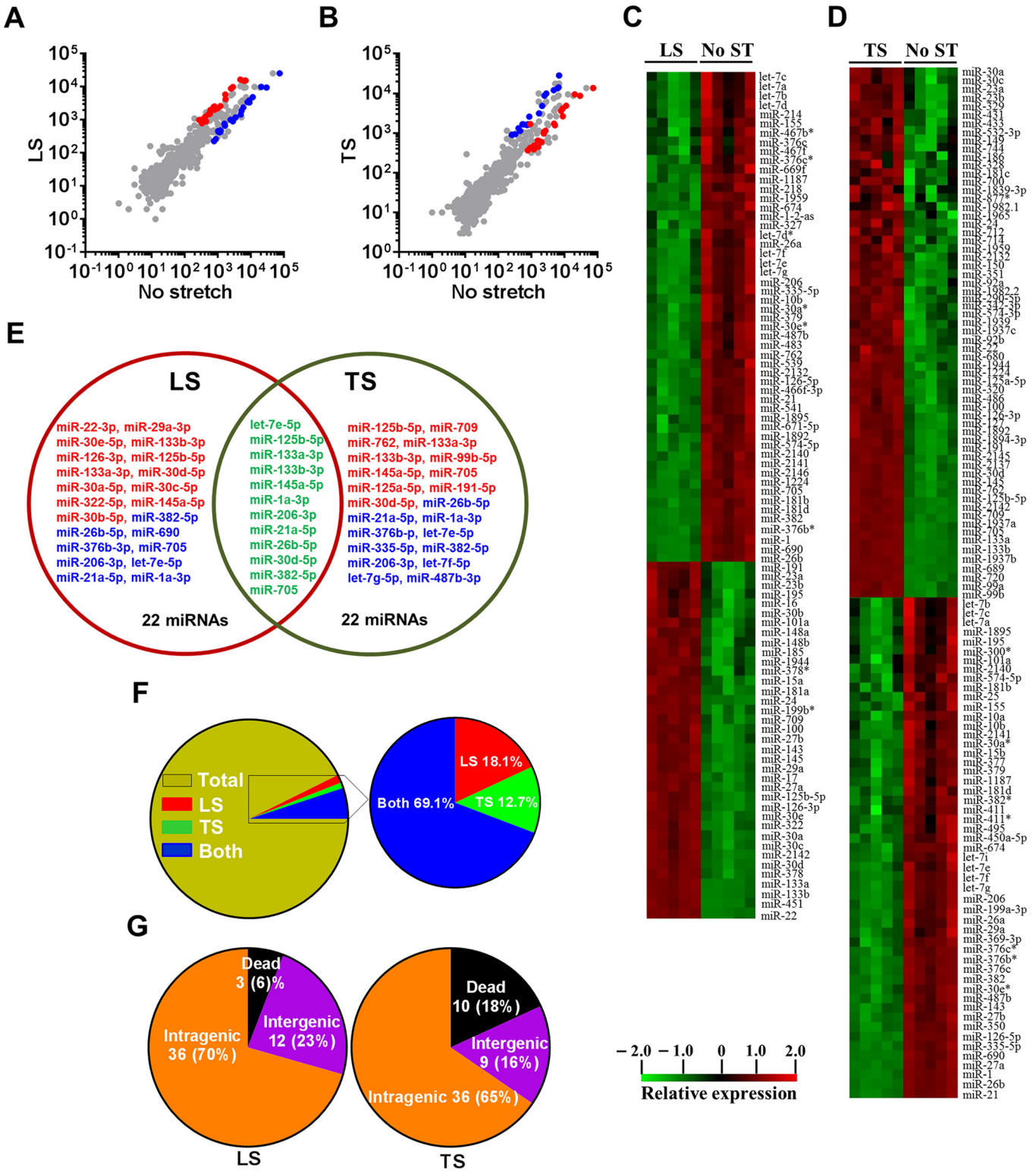

FIGURE 2. **Genome-wide expression profile of mechanomiRs in diaphragm from *mdm* mouse.** Total RNA was isolated from longitudinally or transversely stretched hemidiaphragm from *mdm* mouse and used in miRNA microarray analyses to determine differentially regulated mechanomiRs. *A* and *B*, the scatter plot shows $\log_{10}$-transformed signal intensities for each probe labeled with Cy3 for unstretched (control) and Cy5 for LS (*A*) or TS (*B*) diaphragm. Each *dot* represents one miRNA probe. *C* and *D*, data on the heat map show mechanomiRs differentially expressed in diaphragm in response to LS (*C*) or TS (*D*). *E*, Venn diagram shows up (*red*)- and down (*blue*)-regulated mechanomiRs (>1.5-fold) after stretch. *F*, percentage of differentially expressed mechanomiRs to the total number of miRNAs in the array. *G*, percentage of differentially expressed mechanomiRs based on their genomic location.

Identification of Genome-wide MechanomiRs in Dystrophic Skeletal Muscle—Although other investigators uncovered a role for miRNAs in MDs in both humans (40–43) and mice (44–46), no studies have been designed specifically to uncover a role for mechanomiRs in MDs. In the current study we determined the pattern of regulation of mechanomiRs in dystrophic

TABLE 4
MechanomiRs and their corresponding miRNA gene clusters in diaphragm from WT mouse
Bold indicates differentially regulated mechanomiRs by longitudinal and transverse stretches.

Cluster	Location	miRNA cluster	Differentially expressed mechanomiRs in response to LS	Changes
1	Chr1	miR-199a~214	miR-199a-3p; miR-214-3p	Down
2	Chr1	**miR-206~miR-133b**	**miR-133b-3p; miR-206-3p**	Up/down
3	Chr4	miR-30c1/e/f	miR-30c-5p; miR-30e-5p	Up
4	Chr8	**miR-23a~24~27a**	**miR-23a-3p; miR-24-3p; miR-27a-3p**	Up/down
5	Chr12	**miR-379~410**	**miR-379-5p;** miR-299a-5p; miR-487b-3p; **miR-382-5p; miR-541-5p**	Down
6	Chr15	miR-30b~30d	miR-30b-5p; miR-30d-5p	Up
Total		6 clusters	16 mechanomiRs	
Cluster	**Location**	**miRNA cluster**	**Differentially expressed mechanomiRs in response to TS**	**Changes**
1	Chr1	**miR-206~miR-133b**	**miR-133b-3p; miR-206-3p**	Down/Up
2	Chr8	**miR-23a~24-2~27a**	**miR-23a-3p; miR-27a-3p**	Down
3	Chr12	**miR-379~410**	**miR-541-5p; miR-379-5p;** miR-411-5p; **miR-382-5p**	Down/up
4	Chr12	miR-127~540	miR-127-3p; miR-434-3p	Down
5	Chr13	let-7a1~7d	let-7a-5p; let-7f-5p; let-7d-5p	Down
6	Chr13	miR-23b~27b~24	miR-23b-3p; miR-24-3p; miR-27b-3p	Down
7	Chr15	let-7b~7c	let-7b-5p; let-7c-5p	Up
8	Chr17	miR-99b~let-7e~125a	miR-125a-5p; let-7e-5p	Up
9	Chr18	miR-1~miR133a	miR-1a-3p; miR-133a-3p	Down
10	ChrX	let-7~mir-98	let-7f-5p; miR-98-5p	Up
Total		10 clusters	24 mechanomiRs	

skeletal muscle. We utilized diaphragm muscle from *mdm* mouse and followed the same protocol that we had used to study diaphragm muscle from the WT mouse. As in the WT mouse, the mechanomiRs, expressed at a signal intensity of >500, were 7.8% of the total miRNAs in the array. MechanomiRs that were expressed at the highest signal intensity (>10,000) represented a much smaller fraction of the total miRNAs analyzed (1%). Some of the highly expressed mechanomiRs in *mdm* mice were also myomiRs (*i.e.* miR-1, miR-133a/b, and miR-206), with miR-1 being the most highly expressed miRNA (73,677) followed by miR-206 (29,603). Non-myomiRs such as miR-709 (28,395) and miR-26a (20,464) were also expressed at high signal intensities (Table 6). Of the 700 miRNA probes examined in the stretched and unstretched diaphragms from *mdm* mice (Fig. 2, *A–D*), the array uncovered the induction of 55 differentially regulated mechanomiRs with signal intensity levels of >500 (Table 6). In particular, we identified 10 mechanomiRs in response to LS only, and seven mechanomiRs were identified in response to TS only. In addition, we identified 38 mechanomiRs in response to either LS or TS). Unlike in the WT mouse, LS and TS differentially regulated equal number of mechanomiRs (22 each) at >1.5-fold (Table and Fig. 2*E*). Of 22 mechanomiRs, LS up-regulated 13 and down-regulated nine mechanomiRs and TS up- and down-regulated 11 mechanomiRs independently based on a p value of 0.01. By comparison, LS and TS altered 1.4 and 1% of the mechanomiRs, respectively, among the total miRNAs in the array, suggesting that both directional stretches altered nearly the same number of mechanomiRs in the *mdm* mouse diaphragm (Fig. 2*F*). Interestingly, both LS and TS altered 38 mechanomiRs (5.4%, which is 69% of 55) either in a similar manner or in an opposite manner (Table 6). As in the WT mouse, although some mechanomiRs were regulated by a similar pattern by stretch in both directions, a few mechanomiRs were oppositely regulated by LS and TS. Of note, a subset of mechanomiRs identified previously by other investigators (28) (miR-23b-3p, miR-25, miR-30b-5p, miR-126–3p, miR-143–3p, miR-145a-5p, miR-214, and miR-21a-5p) were also differentially regulated by LS and TS in the *mdm* mouse diaphragm. Taken together, although the diaphragms from WT and *mdm* mice differentially regulated a similar number of mechanomiRs (signal intensity > 500), the *mdm* mouse diaphragms showed a higher number of mechanomiRs; these were regulated >1.5-fold and included most of the previously identified mechanomiRs.

Next, we determined the genomic location of the mechanomiRs in *mdm* mouse diaphragm. We identified that 36 mechanomiRs distinctly induced by LS (70%) and TS (65%) were intragenic miRNAs (Fig. 2*G*), whereas 12 (23%) and nine (16%) mechanomiRs induced by LS and TS, respec-

TABLE 5
MechanomiRs and their families in diaphragm from WT mouse
Bold indicates differentially regulated mechanomiRs by longitudinal and transverse stretches.

No	Family	Differentially expressed mechanomiRs in response to LS	Changes
1	miR-10	miR-125a-5p; miR-125b-5p	Up
2	miR-15	miR-16-5p; miR-195a-5p	Up
3	**miR-26**	**miR-26a-5p; miR-26b-5p**	Down
4	**miR-27**	**miR-27a-3p; miR-27b-3p**	Up
5	miR-30	miR-30a-5p; miR-30b-5p; miR-30c-5p; miR-30d-5p; miR-30e-5p	Up
6	**miR-133**	**miR-133a-3p; miR-133b-3p**	Up
7	miR-154	miR-382-5p; miR-487b-3p	Down
Total	7 families	17 mechanomiRs	
No	**Family**	**Differentially expressed mechanomiRs in response to TS**	**Changes**
1	let-7	let-7a-5p; let-7b-5p; let-7c-5p; let-7d-5p; let-7e-5p; let-7f-5p miR-98-	Up
2	miR-1	5p	Up/down
3	miR-23	miR-1a-3p; miR-206-3p	Down
4	**miR-26**	miR-23a-3p; miR-23b-3p	Up/down
5	**miR-27**	**miR-26a-5p; miR-26b-5p**	Down
6	**miR-133**	**miR-27a-3p; miR-27b-3p**	Down
7	miR-379	**miR-133a-3p; miR-133b-3p;** miR-379-5p; miR-411-5p	Down
Total	7 families	19 mechanomiRs	

tively, were intergenic miRNAs (Fig. 2*G*). We also found 21 clusters of mechanomiR that were transcribed by LS and TS together, in which LS induced the transcription of 12 clusters (containing 30 mechanomiRs) and TS induced the transcription of nine clusters (containing 23 mechanomiRs) (Table 8). Furthermore, LS and TS induced 29 and 26 mechanomiRs, respectively, which fell into 11 and nine families, respectively. Interestingly, except for the miR-15 family, most of the mechanomiR families were induced by both LS and TS (Table 9).

To validate the miRNA microarray data, we measured the expression levels of more than 2.0-fold differentially regulated mechanomiRs by real-time PCR, which confirmed the levels of miR-30e-5p, miR-382–5p, miR-379–5p, miR-763, let-7e-5p, miR-98–5p, miR-22–3p, miR-29a-3p, miR-382–5p, miR-26b-5p, miR-125b-5p, and miR-709 mechanomiRs as more than 2.0-fold (Fig. 3).

Mechanical Stretch Alters miRNA Synthesis Machinery—To explore the mechanism involved in the regulation of mechanomiRs, we investigated the effect of stretch on the expression of key components of the miRNA synthesis machinery. To this end, using real-time PCR we designed primers for selected genes involved in miRNA biogenesis to quantify their expression levels in diaphragms. We found that stretch significantly up-regulated the nuclear protein Drosha, the cytoplasmic protein Dicer1, and the miRNA export protein exportin-5 in diaphragms from WT and *mdm* mice. In contrast, stretch did not affect the expression of DGCR8 in diaphragm from WT mouse, whereas a similar stretch increased DGCR8 in diaphragm from *mdm* mouse (Fig. 4*A*). Next, we determined the expression of the Argonaute proteins, components of the RNA-induced silencing complex (RISC). Although the mRNA levels of Ago2 and Ago5 were significantly higher in diaphragm from WT mouse, diaphragm from *mdm* mouse showed an increased level of Ago1, Ago2, Ago3, and Ago5 in response to stretch (Fig. 4*B*). Interestingly, the overall levels of expression of components of the miRNA synthesis machinery were significantly higher in diaphragm from *mdm* mouse than

TABLE 6

Differentially regulated mechanomiRs in diaphragm from *mdm* mouse

Bold indicates differentially regulated mechanomiRs by longitudinal and transverse stretches. Underlines indicate differentially regulated mechanomiRs at signal intensities > 10,000.

Longitudinal stretch					
No	**MechanomiRs**	**p-value**	**Stretch**	**No Stretch**	**Log_2**
1	miR-22	4.28E-10	1104	197	2.49
2	miR-29a	1.02E-06	1680	434	1.95
3	miR-30e	2.17E-06	997	272	1.87
4	**miR-133b**	3.86E-09	8814	2504	1.82
5	**miR-125b-5p**	5.13E-07	5867	1673	1.81
6	**miR-126-3p**	2.57E-07	16565	4740	1.81
7	**miR-133a**	7.71E-09	9867	2830	1.80
8	**miR-30d**	7.19E-08	1989	583	1.77
9	**miR-30a**	1.35E-06	2445	735	1.73
10	**miR-30c**	5.74E-06	2542	790	1.69
11	miR-322	2.55E-06	1016	327	1.64
12	**miR-145**	9.18E-07	1237	409	1.60
13	miR-30b	5.38E-05	1470	507	1.54
14	**miR-143**	2.39E-07	1522	573	1.41
15	**miR-27a**	9.81E-07	2000	773	1.37
16	**miR-24**	4.01E-09	4237	1705	1.31
17	**miR-23a**	1.40E-04	15099	6168	1.29
18	**miR-191**	2.36E-04	787	328	1.26
19	**miR-378**	1.20E-05	2189	929	1.24
20	**miR-23b**	3.10E-04	15646	6642	1.24
21	**miR-27b**	2.87E-05	2261	986	1.20
22	**miR-709**	4.41E-05	15379	6905	1.16
23	miR-16	5.65E-05	2629	1190	1.14
24	miR-195	6.52E-04	904	437	1.05
25	**miR-382**	7.89E-08	448	2021	-2.17
26	**miR-26b**	2.20E-06	1194	5181	-2.12
27	**miR-690**	4.66E-07	1448	4877	-1.75
28	**miR-376b***	3.86E-07	227	760	-1.74
29	**miR-705**	2.54E-08	264	867	-1.72
30	**miR-206**	4.64E-05	9518	29603	-1.64
31	**let-7e**	7.04E-05	912	2822	-1.63
32	**miR-21**	1.86E-05	1176	3414	-1.54
33	**miR-1**	6.59E-06	25535	73677	-1.53
34	**miR-10b**	3.50E-05	425	1170	-1.46
3536	**let-7g**	4.73E-05	1881	5165	-1.46
37	**let-7f**	4.98E-05	3358	9010	-1.42
38	**miR-487b**	5.81E-05	480	1198	-1.32
39	**miR-335-5p**	1.20E-04	662	1634	-1.30
40	**let-7b**	1.14E-03	2390	5838	-1.29
41	**miR-379**	4.42E-04	1001	2406	-1.27
42	miR-214	7.88E-04	434	1038	-1.26
43	**let-7a**	1.36E-03	4895	11346	-1.21
44	**let-7c**	2.48E-03	3857	8893	-1.21
45	**let-7d**	8.54E-04	3462	7909	-1.19
46	miR-541	6.33E-05	458	1018	-1.15
47	miR-299*	3.70E-03	759	1574	-1.05
48	**miR-26a**	5.45E-04	9985	20464	-1.04
	miR-127	1.86E-03	1872	3386	-0.85

TABLE 6—*continued*

Transverse stretch					
No	**MechanomiRs**	**p-value**	**Stretch**	**No stretch**	**Log_2**
1	**miR-125b-5p**	6.05E-09	9960	1673	2.57
2	**miR-709**	5.93E-09	28395	6905	2.04
3	miR-762	2.02E-06	952	252	1.92
4	**miR-133a**	1.80E-09	9992	2830	1.82
5	**miR-133b**	2.23E-09	8746	2504	1.80
6	miR-99b	2.10E-07	907	260	1.80
7	**miR-145**	3.48E-06	1330	409	1.70
8	**miR-705**	7.18E-07	1669	542	1.62
9	miR-125a-5p	2.58E-04	2594	867	1.58
10	**miR-191**	3.09E-05	952	328	1.54
11	**miR-30d**	6.10E-06	1658	583	1.51
12	**miR-126-3p**	1.62E-05	12005	4740	1.34
13	miR-329	1.25E-03	1139	462	1.30
14	**miR-127**	3.82E-06	4832	2116	1.19
15	**miR-23a**	6.90E-04	13411	6168	1.12
16	**miR-30a**	5.12E-04	1595	735	1.12
17	**miR-23b**	1.35E-03	14162	6642	1.09
18	**miR-30c**	1.51E-03	1678	790	1.09
19	**miR-24**	1.62E-04	3152	1705	0.89
20	**miR-378**	3.95E-03	1680	929	0.85
21	**miR-26b**	1.94E-07	772	5181	-2.75
22	**miR-21**	5.44E-08	576	3414	-2.57
23	**miR-1**	2.58E-08	13680	73677	-2.43
24	**miR-376b***	1.29E-07	161	760	-2.24
25	**let-7e**	8.71E-06	632	2822	-2.16
26	**miR-335-5p**	1.41E-05	447	1634	-1.87
27	**let-7f**	5.70E-06	2659	9010	-1.76
28	**miR-206**	4.97E-05	8741	29603	-1.76
29	**miR-382**	2.15E-07	598	2021	-1.76
30	**let-7g**	6.85E-06	1573	5165	-1.72
31	**miR-487b**	3.05E-06	387	1198	-1.63
32	**miR-690**	3.45E-05	1738	4877	-1.49
33	**miR-27a**	3.00E-05	491	1237	-1.33
34	miR-10b	2.05E-04	466	1170	-1.33
35	miR-199a-3p	1.47E-04	976	2378	-1.28
36	**miR-27b**	5.15E-06	650	1578	-1.28
37	**let-7i**	3.16E-04	1152	2691	-1.22
38	**let-7a**	1.41E-03	4901	11346	-1.21
39	**miR-379**	9.96E-04	1075	2406	-1.16
40	**let-7b**	4.07E-03	2637	5838	-1.15
41	**let-7d**	1.81E-03	3583	7909	-1.14
42	**miR-143**	9.92E-06	423	917	-1.12
43	**miR-26a**	2.03E-04	9458	20464	-1.11
44	**let-7c**	6.61E-03	4141	8893	-1.10
45	miR-25	1.32E-03	366	784	-1.10

those in diaphragm from WT mouse. These data suggest that the higher number of expression of mechanomiRs in diaphragm from *mdm* mouse could be due to the enhanced

TABLE 7

Differentially regulated mechanomiRs (>1.5-fold) in diaphragm from *mdm* mouse

Bold indicates differentially regulated mechanomiRs by longitudinal and transverse stretches. Underlines indicate differentially regulated mechanomiRs at signal intensities > 10,000.

Longitudinal stretch						Transverse stretch					
No	MechanomiRs	p-value	Stretch	No stretch	Log_2	No	MechanomiRs	p-value	Stretch	No stretch	Log_2
1	miR-22-3p	4.28E-10	1104	197	2.49	1	**miR-125b-5p**	6.05E-09	9960	1673	2.57
2	miR-29a-3p	1.02E-06	1680	434	1.95	2	miR-709	5.93E-09	28395	6905	2.04
3	miR-30e-5p	2.17E-06	996	272	1.87	3	miR-762	2.02E-06	952	252	1.92
4	**miR-133b-3p**	3.86E-09	8814	2504	1.82	4	**miR-133a-3p**	1.80E-09	9992	2830	1.82
5	miR-126-3p	2.57E-07	16564	4740	1.81	5	**miR-133b-3p**	2.23E-09	8745	2504	1.80
6	**miR-125b-5p**	5.13E-07	5867	1673	1.81	6	miR-99b-5p	2.10E-07	907	260	1.80
7	**miR-133a-3p**	7.71E-09	9867	2830	1.80	7	**miR-145a-5p**	3.48E-06	1329	409	1.70
8	**miR-30d-5p**	7.19E-08	1988	583	1.77	8	**miR-705**	7.18E-07	1668	542	1.62
9	miR-30a-5p	1.35E-06	2444	735	1.73	9	miR-125a-5p	2.58E-04	2593	867	1.58
10	miR-30c-5p	5.74E-06	2542	790	1.69	10	miR-191-5p	3.09E-05	952	328	1.54
11	miR-322-5p	2.55E-06	1016	327	1.64	11	**miR-30d-5p**	6.10E-06	1657	583	1.51
12	**miR-145a-5p**	9.18E-07	1236	409	1.60	12	**miR-26b-5p**	1.94E-07	772	5180	-2.75
13	miR-30b-5p	5.38E-05	1470	507	1.54	13	**miR-21a-5p**	5.44E-08	576	3414	-2.57
14	**miR-382-5p**	7.89E-08	448	2020	-2.17	14	**miR-1a-3p**	2.58E-08	13680	73676	-2.43
15	**miR-26b-5p**	2.20E-06	1194	5180	-2.12	15	miR-376b-p	1.29E-07	161	760	-2.24
16	miR-690	4.66E-07	1448	4876	-1.75	16	**let-7e-5p**	8.71E-06	632	2822	-2.16
17	miR-376b-3p	3.86E-07	227	760	-1.74	17	miR-335-5p	1.41E-05	447	1633	-1.87
18	**miR-705**	2.54E-08	264	867	-1.72	18	**miR-382-5p**	2.15E-07	598	2020	-1.76
19	**miR-206-3p**	4.64E-05	9518	29603	-1.64	19	**miR-206-3p**	4.97E-05	8741	29603	-1.76
20	**let-7e-5p**	7.04E-05	912	2822	-1.63	20	let-7f-5p	5.70E-06	2659	9009	-1.76
21	**miR-21a-5p**	1.86E-05	1176	3414	-1.54	21	let-7g-5p	6.85E-06	1573	5164	-1.72
22	**miR-1a-3p**	6.59E-06	25535	73676	-1.53	22	miR-487b-3p	3.05E-06	387	1198	-1.63

activation of number of specific players of the miRNA synthesis machinery.

Identification of MechanomiR-regulated Predicted Biological Pathways in WT and mdm Mice—To determine the genome-wide mechanomiR-regulated predicted biological pathways in diaphragms from WT and *mdm* mice, we first combined both the LS- and TS-regulated mechanomiRs of WT or *mdm* mice. As a result, the WT and *mdm* mice totally regulated 51 and 55 mechanomiRs, respectively, at a signal intensity of >500 (Fig. 5*A*). However, with regard to highly differentially expressed mechanomiRs (>1.5-fold), WT and *mdm* mice regulated 29 and 31 mechanomiRs, respectively (Fig. 5*B*). As the mechanomiR numbers were still higher, we selected >2.0-fold differentially regulated mechanomiRs from WT and *mdm* mice for further analysis. As a result, we found that diaphragm muscle from WT mouse differentially regulated five mechanomiRs at >2.0-fold (three up-regulated and two down-regulated), whereas diaphragm from *mdm* mouse differentially regulated nine mechanomiRs at >2.0-fold (three up-regulated and six down-regulated). However, only two mechanomiRs (let-7e and miR-382) were found to be commonly regulated in both WT and *mdm* mice (Fig. 5*C*). To determine the mechanomiR-regulated biological pathways, we used DIANA miRPath v 2.0 software. The threshold *p* values for the pathway and MicroT were set to 0.05 and 0.8, respectively, and the KEGG pathway in DIANA miRPath identified 41 (Table 10) and 74 (Table 11) mechanomiR-regulated biological pathways for WT and *mdm* mice, respectively. In addition, 28 pathways were common for both WT and *mdm* mice (Fig. 5*D*). Among those pathways, 19 (WT) and 32 (*mdm*) pathways were associated with skeletal muscle functions. In addition, our data showed only five and 18 skeletal muscle-associated pathways that were unique to WT and *mdm* mice, respectively, and 14 pathways were common for both WT and *mdm* mice (Fig. 5*D*). According to gene ontology, there are 36 genes are involved in the five pathways in WT mouse (Fig. 5*E*), whereas 251 gene are involved in 18 pathways in *mdm* mouse (Fig. 5*F*). Although both WT and *mdm* mice shared 14 different pathways, the involvement and appearance of genes in each pathway were higher in diaphragm muscle from *mdm* mouse (Fig. 6, *A* and *B*). For example, the PI3-Akt

TABLE 8

MechanomiRs and their corresponding miRNA gene clusters in diaphragm from *mdm* mouse

Bold indicates differentially regulated mechanomiRs by longitudinal and transverse stretches. Underlines indicate differentially regulated mechanomiRs at signal intensities > 10,000.

Cluster	Location	miRNA cluster	Differentially expressed mechanomiRs in response to LS	Changes
1	Chr6	miR-29a~29b-1	miR-29a-3p; miR-29b-3p	Up/down
2	Chr4	miR-30f~30e~30c-1	miR-30e; miR-30c-5p	Up
3	Chr1	**miR-206~133b**	**miR-133b-3p; miR-206-3p**	Up/down
4	Chr2	**miR-1a-1~133a-2**	**miR-1a-3p; miR-133a-3p**	Up/down
5	Chr15	miR-30d~30b	miR-30d-5p; miR-30b-5p	Up
6	Chr18	**miR-143~145a**	**miR-145a-5p; miR-143-3p**	Up
7	Chr8	**miR-23a~27a~24-2**	**miR-23a-3p; miR-27a-3p; miR-24-3p**	Up
8	Chr13	**miR-23b~27b~24-1**	**miR-23b-3p; miR-27b-3p**	Up
9	Chr12	**miR-379~410**	**miR-379-5p;** miR-299-5p; **miR-376-5p; miR-487b-3p; miR-382-5p;** miR-541-5p	Down
10	Chr1	**miR-206~133b**	**miR-133b-3p; miR-206-3p**	Up/down
11	Chr15	**let-7b~7c**	**let-7b-5p; let-7c-5p**	Down
12	Chr13	**let-7a~7f-7d**	**let-7a-5p; let-7f-5p; let-7d-5p**	Down
Total		12 clusters	30 mechanomiRs	
Cluster	**Location**	**miRNA cluster**	**Differentially expressed mechanomiRs in response to TS**	**Changes**
1	Chr17	miR-99b~125~let-7e	miR-99b-5p; miR-125a-5p; let-7e-5p	Up/down
2	Chr12	**miR-379~410**	**miR-379-5p; miR-376-5p; miR-487b-3p; miR-382-5p**	Down
3	Chr1	**miR-206~133b**	**miR-133b-3p; miR-206-3p**	Up/down
4	Chr2	**miR-1a-1~133a-2**	**miR-1a-3p; miR-133a-3p**	Up/down
5	Chr18	**miR-143~145a**	**miR-145a-5p; miR-143-3p**	Up/down
6	Chr8	**miR-23a~27a~24-2**	**miR-23a-3p; miR-27a-3p; miR-24-3p**	Up/down
7	Chr13	**miR-23b~27b~24-1**	**miR-23b-3p; miR-27b-3p**	Up/down
8	Chr15	**let-7b~7c**	**let-7b-5p; let-7c-5p**	Down
9	Chr13	**let-7a~7f-7d**	**let-7a-5p; let-7f-5p; let-7d-5p**	Down
Total		9 clusters	23 mechanomiRs	

and MAP kinase signaling pathways involve nearly twice the number of genes in the *mdm* mouse compared with those in the WT mouse (Fig. 6*A*). Next, we determined the let-7e-5p-predicted biological pathways in WT and *mdm* mice. DIANA miRPath provided 24 predicted pathways (Table 12), including 18 skeletal muscle-specific pathways (Fig. 6*C*). Interestingly, miR-98–5p was highly up-regulated in diaphragm muscle from WT mouse, but its mechanosensitivity was lost in diaphragm muscle from *mdm* mouse, which led us to explore miR-98–5p-predicted biological pathways. DIANA miRPath provided 26 predicted pathways (Table 13), among which were 18 pathways that are skeletal muscle-specific (Fig. 6*D*). Finally, we compared the differentially regulated mechanomiRs of *mdm* diaphragm with the differentially regulated miRNAs of the *mdx* skeletal muscle. As shown in Fig. 6*E*, nine differentially regulated miRNAs in *mdx* skeletal muscle were mechanomiRs that were identified in both WT and *mdm* mice. However, most of the mechanomiRs identified in the present study were regulated in an opposite manner to that in the skeletal muscles of *mdx* mice.

Dysregulation of the MechanomiR-let-7e-5p in mdm Mouse Increases ECM Proteins—Interestingly, let-7e-5p is the only mechanomiR that is highly regulated in an opposite manner between the diaphragms of WT and *mdm* mice. Therefore, we focused our study on determining whether let-7e-5p is potentially involved in the progression of MD in *mdm* mouse. Although the DIANA miRPath identified 18 pathways related to skeletal muscle functions, ECM-receptor interaction was ranked first (Table 10). Many lines of evidence have shown that the up-regulation of ECM proteins in dystrophic skeletal muscle plays a key role in the development of fibrosis, a hallmark of dystrophic skeletal muscle (47). In the present study, we found that let-7e-5p was highly down-regulated in diaphragm from *mdm* mouse. These data are consistent with our hypothesis that fibrosis in the skeletal muscles from the *mdm* mice is caused, at least in part, by let-7e-5p-mediated up-regulation of ECM proteins. To further test our hypothesis, we first determined whether let-7e-5p transcriptionally or post-transcriptionally suppressed endogenous ECM gene expressions. To do this, we

TABLE 9
MechanomiRs and their families in diaphragm from *mdm* mouse
Bold indicates differentially regulated mechanomiRs by longitudinal and transverse stretches.

No	Family	Differentially expressed mechanomiRs in response to LS	Changes
1	**let-7**	**let-7a-5p; let-7b-5p; let-7c-5p; let-7d-5p; let-7e-5p; let-7f-5p**	Down
2	**miR-10**	**miR-10b-5p; miR-125b-5p**	Up/down
3	miR-15	miR-16-5p; miR-195a-5p	Up
4	**miR-133**	**miR-133a-3p; miR-133b-3p**	Up
5	**miR-30**	**miR-30a-5p;** miR-30b-5p; **miR-30c-5p; miR-30d-5p**; miR-30e-5p	Up
6	**miR-27**	**miR-27a-3p; miR-27b-3p**	Up
7	**miR-23**	**miR-23a-3p; miR-23b-3p**	Up
8	**miR-15**	**miR-16-5p; miR-195a-5p**	Up
9	**miR-154**	**miR-382-5p; miR-487b-3p**	Down
10	**miR-26**	**miR-26a-5p; miR-26b-5p**	Down
11	**miR-1**	**miR-1a-3p; miR-206-3p**	Down
Total	11	29 mechanomiRs	
No	**Family**	**Differentially expressed mechanomiRs in response to TS**	**Changes**
1	**let-7**	**let-7a-5p; let-7b-5p; let-7c-5p; let-7d-5p; let-7e-5p; let-7f-5p;** let-7i	Down
2	**miR-10**	**miR-10b-5p**; miR-99b-5p; miR-125a-5p; **miR-125b-5p**	Up/down
3	**miR-133**	**miR-133a-3p; miR-133b-3p**	Up
4	**miR-30**	**miR-30a-5p;** m**miR-30c-5p; miR-30d-5p**	Up
5	**miR-27**	**miR-27a-3p; miR-27b-3p**	Down
6	**miR-23**	**miR-23a-3p; miR-23b-3p**	Up
7	**miR-154**	**miR-382-5p; miR-487b-3p**	Down
8	**miR-26**	**miR-26a-5p; miR-26b-5p**	Down
9	**miR-1**	**miR-1a-3p; miR-206-3p**	Down
Total	9	26 mechanomiRs	

isolated primary myoblasts from WT mouse diaphragm (pMB^{wt}) and stably transfected them with either a pEGP empty vector or a pEGP-let-7e-5p vector. pMB^{wt} carrying pEGP-let-7e-5p showed nearly a 3-fold overexpression of let-7e-5p (Fig. 6*F*). To determine the expression of ECM genes in pMB^{wt} overexpressing let-7e-5p, we isolated total RNA from pEGP or pEGP-let-7e-5p-transfected pMB^{wt} and used it in a custom-made PCR array having 87 genes related to ECM proteins. The array identified that overexpression of let-7e-5p significantly decreased expression of *Col1a1*, *Col1a2*, *Col3a1*, *Col24a1*, *Col27a1*, *Itga1*, *Itga4*, *Scd1*, and *Thbs1* mRNAs by more than 2-fold (Fig. 7*A*), suggesting that let-7e-5p targets at least those nine mRNAs of ECM gene. Second, we examined whether stretch could alter the expression of let-7e-5p and its target ECM genes *in vitro*. To do this, we stretched pMB^{wt} or pMB^{mdm} as described under "Experimental Procedures." Interestingly, although stretch significantly decreased *Col1a1, Col1a2, Col3a1, Col24a1, Col27a1, Itga1, Itga4, Scd1,* and *Thbs1* mRNA levels in pMB^{wt}, a similar stretch increased the mRNA levels of these genes in pMB^{mdm} (Fig. 7*B*). Likewise, let-7e-5p expres-

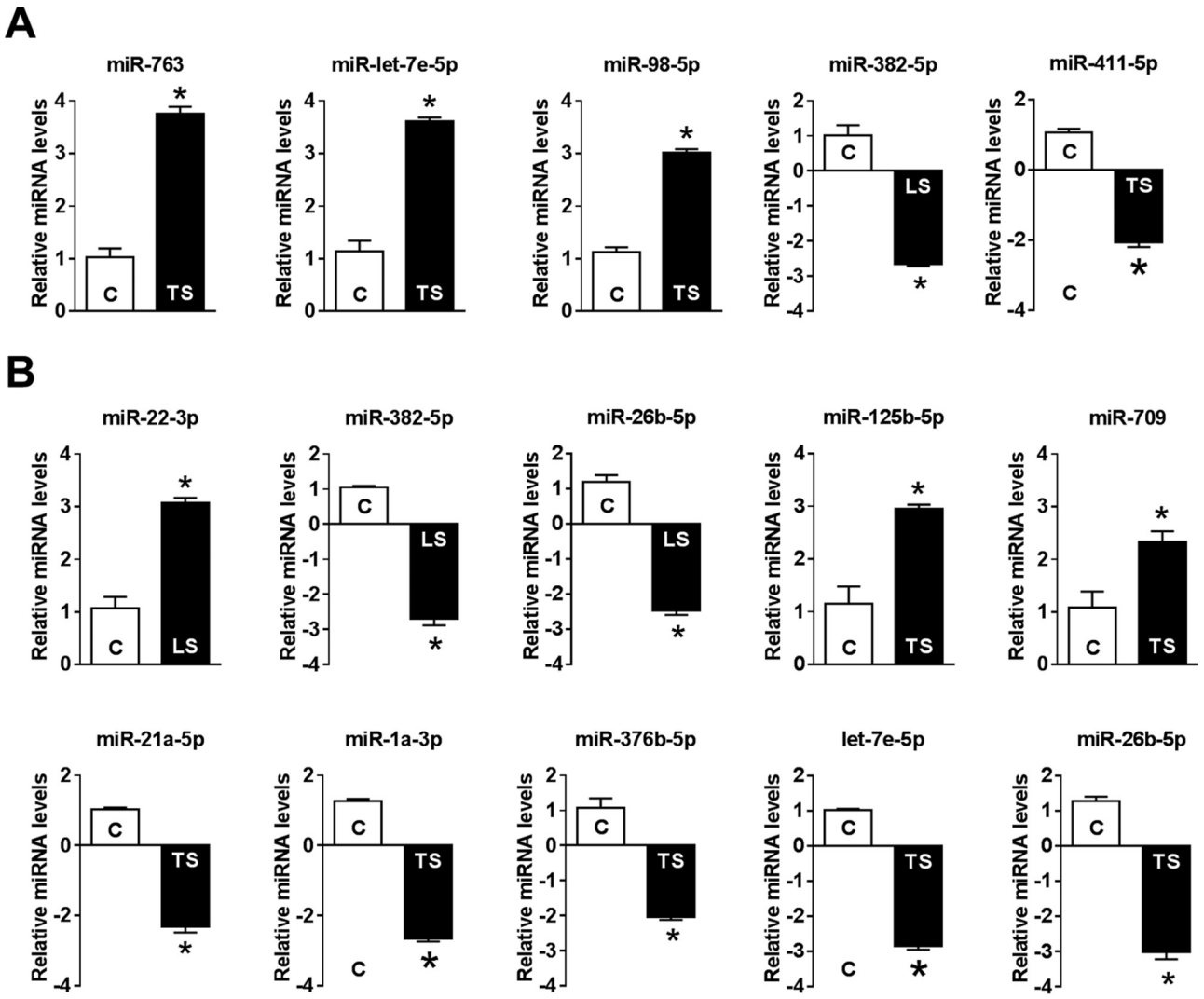

FIGURE 3. **Quantification of mechanomiRs by real-time PCR.** A portion of RNA used in the microarray was used in real-time PCR to confirm the expression level of mechanomiRs that were differentially regulated >1.9-fold in the microarray. Shown is the expression level of mechanomiRs in diaphragms from WT (*A*) and *mdm* (*B*) mice. Each *bar* represents mean ± S.E. ($n = 3$). *, $p < 0.05$.

sion was also regulated in an opposite manner between pMB^{wt} and pMB^{mdm} (Fig. 7*C*). These results provide the first experimental evidence of a negative correlation between let-7e-5p and ECM gene expressions in myocytes from WT and *mdm* mice. To confirm whether the stretch-induced down-regulation of ECM genes in pMB^{wt} was due to the mechanomiR let-7e-5p, we inhibited let-7e-5p in pMB^{wt} with let-7e-5p antagomir. Although the stretching of pMB^{wt} significantly decreased ECM gene expressions, the transfection of pMB^{wt} with let-7e-5p antagomir abolished the stretch-induced ECM gene expression (Fig. 8*A*). To further confirm that let-7e-5p-regulated ECM gene expressions, we overexpressed let-7e-5p in pMB^{mdm} with a pEGP-let-7e-5p construct. Although stretch up-regulated ECM gene expression in pMB^{mdm}, transfection of the let-7e-5p overexpression construct dramatically decreased the stretch-induced ECM gene expression profile (Fig. 8*B*). Finally, we sought to determine the expression of let-7e-5p targeting ECM proteins in WT and *mdm* mouse diaphragms. As expected, whereas stretch down-regulated the ECM proteins Col1a1, Col1a2, Col3a1, Col24a1, Col27a1, Itga1, Itga4, Scd1, and Thbs1 in diaphragm muscle from WT mouse, similar stretch up-regulated those ECM protein from *mdm* mouse. Overall, these data confirmed that mechanomiR let-7e-5p is accountable for the up-regulation of ECM proteins in the diaphragm muscle from *mdm* mouse.

Diaphragm from mdm Mouse Displays Up-regulation of TGF-β1 Pathway—Studies have shown an increased expression of TGF-β1 gene in skeletal muscles from *mdx* mice (48–50) and DMD patients (51). Other investigators have demonstrated that activated TGF-β signaling in dystrophic muscles in DMD patients is associated with impaired muscle regeneration and increased fibrosis (51, 52). However, the regulation of TGF-β1 signaling in skeletal muscles from *mdm* mice is unknown. In the current study, we determined whether stretch could alter the expression of TGF-β1 in diaphragm muscle. As shown in Fig. 9, although stretch reduced TGF-β1 levels in diaphragm muscle from WT mouse (Fig. 9*A*), similar stretch enhanced TGF-β1 levels in diaphragm muscle from *mdm* mouse (Fig. 9*B*). It is well documented that TGF-β1-induced gene transcription is mediated by intracellular substrates

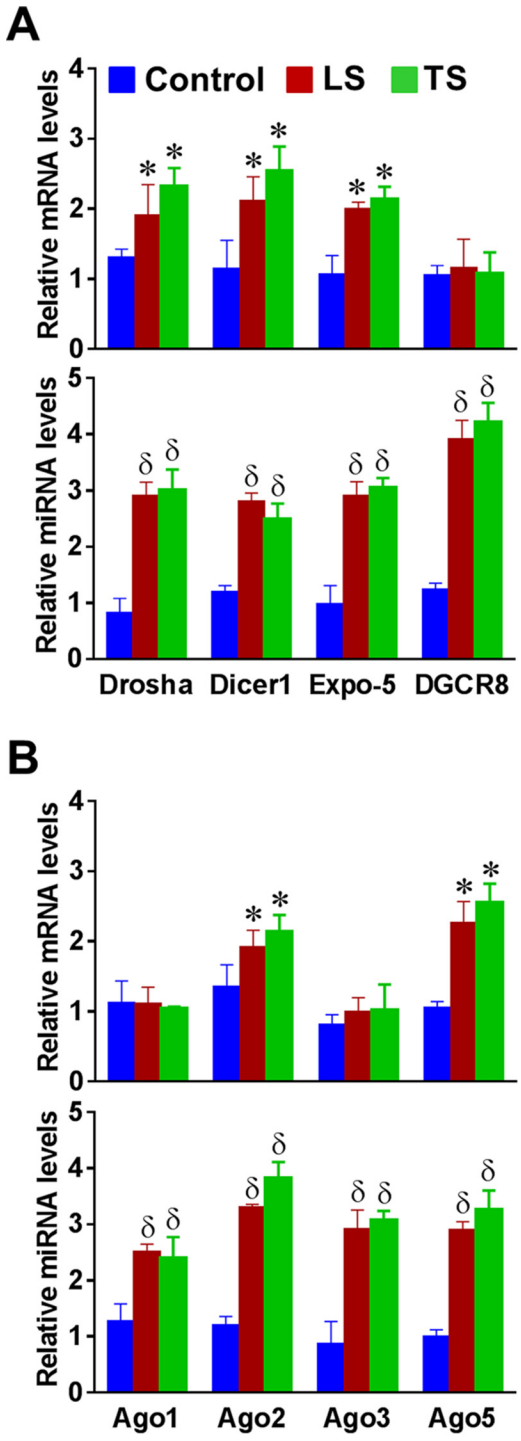

FIGURE 4. **Mechanical stretch up-regulates miRNA synthesis machinery.** Total RNA was isolated from control (no stretch), longitudinally stretched or transversally stretched hemidiaphragms from WT or *mdm* (*bottom panels* in *A* and *B*) mice and used in real-time PCR to determine the expression levels of selected genes that control miRNA biogenesis. Each *bar* represents mean ± S.E. ($n = 4$). *, $p < 0.05$ *versus* control diaphragm from WT mouse. δ, $p < 0.05$ *versus* control diaphragm from *mdm* mouse.

known as SMADs (53). Therefore, we sought to determine the expressions of SMAD2 and SMAD3 proteins in response to stretch. Stretching of the diaphragm decreased the phosphorylation of SMAD2/SMAD3 proteins in WT mouse (Fig. 9*C*). In contrast, stretch elevated the phosphorylation of SMAD2 and SMAD3 proteins in diaphragm muscle from *mdm* mouse (Fig. 9*B*), suggesting an opposite regulation of TGF-β1 and activation of SMAD proteins between WT and *mdm* mice.

MechanomiR-98 Negatively Regulates Myoblast Differentiation—We have shown previously that mechanical stretch inhibits differentiation of C2C12 myoblasts (6). To determine whether let-7e-5p and/or miR-98–5p may play a role in controlling the stretch-induced inhibition of myoblast differentiation, we transfected pMB^{wt} with let-7e-5p and/or miR-98–5p antagomirs and cultured them in differentiation medium with stretch for 1 h every 24 h for 5 days. First, we determined whether each antagomir effectively inhibited the respective endogenous mechanomiR. As shown in Fig. 10*A*, transfection of pMB^{wt} with let-7e-5p and miR-98–5p antagomirs efficiently decreased the stretch-increased endogenous let-7e-5p and miR-98–5p levels, respectively, suggesting the specificity and efficacy of antagomirs. As expected, culture of pMB^{wt} in differentiation medium for 5 days displayed the differentiation of most of the myoblasts into myotubes (Fig. 10*B*). In agreement with our previous findings (6), stretching pMB^{wt} in differentiation medium for 5 consecutive days reduced the formation of myotubes (Fig. 10*C*). Interestingly, pMB^{wt} transfected with both antagomirs or with miR-98–5p alone, induced myoblast differentiation in the presence of stretch (Fig. 10*C*), confirming that miR-98–5p, but not let-7e-5p, regulates the stretch-induced inhibition of myoblast differentiation. These studies also suggest that although let-7e-5p and miR-98–5p belong to the same family with almost identical sequences and synergistically up-regulated by stretch, their biological functions are distinct, at least in their roles in the myoblast differentiation program.

Discussion

In this study, we tested the hypothesis that the dysregulation of mechanomiRs in dystrophic skeletal muscle plays key role in the progression of disease. We conducted a comprehensive miRNA analysis on mechanically stretched and unstretched diaphragm muscles from WT and *mdm* mice using miRNA microarrays, followed by bioinformatics analyses to determine the predicted target genes of mechanomiRs and their biological pathways. The predicted mechanomiR target genes were validated by gain-of-function and loss-of-function studies. We found that mechanical stretch significantly altered miRNA expression profile in diaphragms from WT and *mdm* mice compared with unstretched diaphragms. Some of the mechanomiRs were previously identified as mechanosensitive miRNAs in endothelial cells (27, 28). Interestingly, although stretch altered (> 500 signal intensity) almost equal number of mechanomiRs between WT and *mdm* mice, number of highly expressed mechanomiRs (>2-fold) were more in *mdm* mice than those in WT mice. Among the highly expressed mechanomiRs (> 2.0-fold), let-7e-5p was the only mechanomiR found to be regulated in an opposite manner between WT and *mdm* mice. Our data provide experimental evidence that let-7e-5p targets the ECM genes *Col1a1*, *Col1a2*, *Col3a1*, *Col24a1*, *Col127a1*, *Itga1*, *Itga4*, *Scd1*, and *Thbs1* as evidenced by real-time PCR and Western blot analyses, and gain-of-function and loss-of-function experiments. In addition, stretch up-regulated mechanomiR-98–5p in diaphragm from WT mouse, but not in

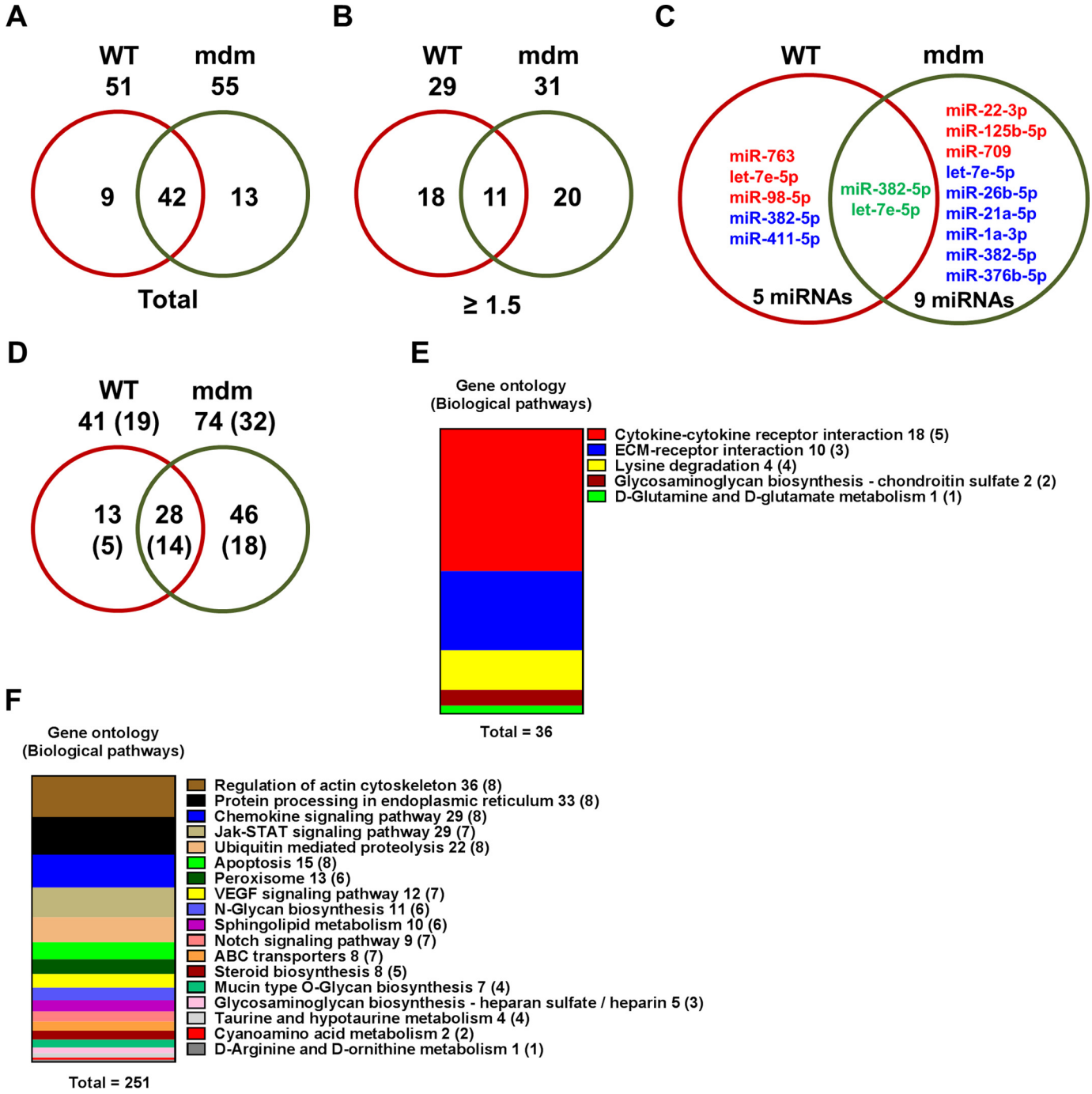

FIGURE 5. **Genome-wide mechanomiR-regulated predicted biological pathways in WT and *mdm* mice.** *A* and *B*, Venn diagram shows number of mechanomiR-regulated biological pathways. *Numbers* outside the *circles* indicate the number of pathways regulated by mechanomiRs at signal intensity >500 (*A*) or ≥1.5-fold (*B*) in WT or *mdm* mice. Similarly, the *numbers* inside the *circles* indicate the total number of pathways regulated by mechanomiRs unique to WT or *mdm* mice or in both phenotypes. *C* and *D*, number of mechanomiRs regulated by LS and TS at ≥2.0-fold in WT or *mdm* mice or in both phenotypes (*C*) and their biological pathways (*D*). *Numbers* outside the *circles* indicate the number of pathways, and *numbers* inside the *circles* indicate the number of pathways unique to WT or *mdm* mice or in both phenotypes. The *numbers* in *parentheses* indicate the number of skeletal muscle-specific pathways. *E* and *F*, gene ontology of mechanomiR-regulated pathways in WT (*E*) and *mdm* (*F*) mice. *Numbers outside* and *inside* the parenthesis indicate the number of genes and mechanomiRs, respectively, associated with each pathway.

diaphragm from *mdm* mouse. We identified a novel role for miR-98–5p as a negative regulator of myoblast differentiation program. Finally, we showed overactivation of TGF-β1/SMAD signaling pathway in diaphragm from *mdm* mouse. These results provide the first experimental evidence that the dysregulation of mechanomiRs and their target gene regulatory networks in dystrophic skeletal muscle contributes, at least in part, to disease progression in MD, at least in the *mdm* mouse model of MD.

Controlled regulation of ECM proteins during skeletal muscle growth and repair is critical in providing a scaffold to build and structure new muscles. However, the excessive or uncontrolled deposition of ECM proteins leads to fibrosis, which progressively deteriorates locomotor capacity, posture mainte-

TABLE 10

Biological pathways regulated by mechanomiRs (>2.0-fold) in diaphragm from WT mouse

Bold indicates pathways commonly regulated by mechanomiRs between WT and *mdm* mice; italics indicate skeletal muscle-specific pathways; and underlines indicate pathways unique to WT mouse diaphragm.

No	KEGG pathway	p-value	#genes	#miRNAs
1	*ECM-receptor interaction*	*9.49E-12*	*10*	*3*
2	Long-term potentiation	5.32E-07	12	5
3	***Insulin signaling pathway***	***7.56E-07***	***18***	***4***
4	***Wnt signaling pathway***	***1.86E-06***	***19***	***5***
5	***mTOR signaling pathway***	***4.09E-06***	***11***	***5***
6	***ErbB signaling pathway***	***1.07E-05***	***12***	***4***
7	***MAPK signaling pathway***	***2.21E-05***	***25***	***5***
8	Melanogenesis	0.000134754	13	4
9	***Adherens junction***	***0.000410593***	***10***	*4*
10	***Focal adhesion***	***0.000410593***	***19***	***4***
11	***Neurotrophin signaling pathway***	***0.000410593***	***13***	***5***
12	*Valine, leucine and isoleucine degradation*	*0.000410593*	*5*	*5*
13	Endometrial cancer	0.000505508	7	4
14	Amoebiasis	0.000554939	11	4
15	Glioma	0.000651998	9	4
16	***PI3K-Akt signaling pathway***	***0.000651998***	***28***	***5***
17	Basal cell carcinoma	0.000780101	8	4
18	Axon guidance	0.001057085	15	4
19	*Glycosaminoglycan biosynthesis - chondroitin sulfate*	*0.001958405*	*2*	*2*
20	Transcriptional misregulation in cancer	0.003667373	17	5
21	Oocyte meiosis	0.004533368	12	5
22	SNARE interactions in vesicular transport	0.004533368	5	3
23	Acute myeloid leukemia	0.004586797	7	5
24	Thyroid cancer	0.005308488	4	4
25	*Protein digestion and absorption*	*0.006479882*	*9*	*2*
26	Synaptic vesicle cycle	0.006632759	6	4
27	*Valine, leucine and isoleucine biosynthesis*	*0.007465197*	*1*	*2*
28	T cell receptor signaling pathway	0.01125153	10	4
29	***Calcium signaling pathway***	***0.01182387***	***15***	***4***
30	***Hedgehog signaling pathway***	***0.01182387***	***6***	***3***
31	Prostate cancer	0.01182387	9	4
32	*Cytokine-cytokine receptor interaction*	*0.01424332*	*18*	*5*
33	*Lysine degradation*	*0.01523289*	*5*	*4*
34	Amphetamine addiction	0.01560699	9	3
35	Pathways in cancer	0.01993422	23	5
36	***TGF-beta signaling pathway***	***0.01993422***	***9***	***4***
37	***Type II diabetes mellitus***	***0.02590973***	***5***	***3***
38	*D-Glutamine and D-glutamate metabolism*	*0.03781549*	*1*	*1*
39	***Lipoic acid metabolism***	***0.03781549***	***1***	***2***
40	Progesterone-mediated oocyte maturation	0.0380444	8	5
41	Chronic myeloid leukemia	0.03991234	7	4

TABLE 11

Biological pathways regulated by mechanomiRs (>2.0-fold) in diaphragm from *mdm* mouse

Bold indicates pathways commonly regulated by mechanomiRs of WT and *mdm* mice; italics indicate skeletal muscle-specific pathways; and underlines indicate pathways unique to *mdm* mouse diaphragm.

No	KEGG pathway	p-value	#genes	#miRNAs
1	**MAPK signaling pathway**	**1.18E-13**	**56**	**9**
2	**mTOR signaling pathway**	**1.42E-11**	**21**	**8**
3	Axon guidance	1.48E-08	33	9
4	**PI3K-Akt signaling pathway**	**1.48E-08**	**60**	**8**
5	***Wnt signaling pathway***	***3.85E-08***	***35***	***9***
6	*Steroid biosynthesis*	*1.26E-07*	*8*	*5*
7	Prostate cancer	4.08E-07	21	9
8	**ErbB signaling pathway**	**3.23E-06**	**20**	**7**
9	Long-term potentiation	2.77E-05	16	8
10	*Protein processing in endoplasmic reticulum*	*3.94E-05*	*33*	*8*
11	Hypertrophic cardiomyopathy (HCM)	4.31E-05	18	7
12	**Neurotrophin signaling pathway**	**4.31E-05**	**24**	**8**
13	*Mucin type O-Glycan biosynthesis*	*4.65E-05*	*7*	*4*
14	**Insulin signaling pathway**	**5.72E-05**	**26**	**8**
15	Endocytosis	0.000148	38	8
16	Endometrial cancer	0.000148	12	8
17	**Focal adhesion**	**0.000148**	**34**	**9**
18	*Regulation of actin cytoskeleton*	*0.000154*	*36*	*8*
19	Bacterial invasion of epithelial cells	0.000196	15	9
20	*N-Glycan biosynthesis*	*0.000324*	*11*	*6*
21	Protein digestion and absorption	0.000402	17	7
22	Acute myeloid leukemia	0.000434	13	8
23	**Calcium signaling pathway**	**0.000434**	**31**	**8**
24	Circadian rhythm	0.000434	9	7
25	**Lipoic acid metabolism**	**0.000661**	**2**	**2**
26	Transcriptional misregulation in cancer	0.000661	33	9
27	*Jak-STAT signaling pathway*	*0.0009*	*26*	*7*
28	Glioma	0.000909	15	8
29	Dilated cardiomyopathy	0.000958	17	7
30	*Taurine and hypotaurine metabolism*	*0.001503*	*4*	*4*
31	Chronic myeloid leukemia	0.001543	15	7
32	Pathways in cancer	0.001543	48	9
33	Fc gamma R-mediated phagocytosis	0.001572	17	9
34	Small cell lung cancer	0.001588	16	8
35	**TGF-beta signaling pathway**	**0.001894**	**17**	**7**
36	Melanoma	0.001982	14	8
37	**Adherens junction**	**0.002621**	**17**	**8**
38	Melanogenesis	0.003987	18	8
39	Renin-angiotensin system	0.004254	5	3
40	Thyroid cancer	0.005044	7	7
41	*Chemokine signaling pathway*	*0.008998*	*29*	*8*
42	Endocrine and other factor-regulated calcium reabsorption	0.010004	10	8
43	Long-term depression	0.010004	12	7
44	mRNA surveillance pathway	0.010004	17	6
45	*VEGF signaling pathway*	*0.010004*	*12*	*7*
46	Bladder cancer	0.010339	9	6
47	Glutamatergic synapse	0.010732	19	8
48	Arrhythmogenic right ventricular cardiomyopathy (ARVC)	0.010818	15	7
49	Osteoclast differentiation	0.011542	20	8
50	T cell receptor signaling pathway	0.012591	18	7
51	HTLV-I infection	0.013038	41	9
52	Dopaminergic synapse	0.014908	22	7
53	Aldosterone-regulated sodium reabsorption	0.015367	8	7
54	Hepatitis B	0.015367	24	8
55	*Ubiquitin mediated proteolysis*	*0.021135*	*22*	*8*
56	Colorectal cancer	0.02452	11	8
57	*Notch signaling pathway*	*0.02452*	*9*	*7*
58	Chagas disease (American trypanosomiasis)	0.027616	17	8
59	*Cyanoamino acid metabolism*	*0.027616*	*2*	*2*
60	Dorso-ventral axis formation	0.027616	5	4
61	**Hedgehog signaling pathway**	**0.029119**	**9**	**5**
62	*Apoptosis*	*0.029945*	*15*	*8*
63	African trypanosomiasis	0.030888	7	5
64	*D-Arginine and D-ornithine metabolism*	*0.031482*	*1*	*1*
65	HIF-1 signaling pathway	0.032819	18	8
66	Basal cell carcinoma	0.036638	10	7
67	Legionellosis	0.036638	10	8
68	*Peroxisome*	*0.036638*	*13*	*6*
69	Influenza A	0.03686	24	9
70	*Sphingolipid metabolism*	*0.039206*	*10*	*6*
71	Fc epsilon RI signaling pathway	0.039428	12	6
72	*Glycosaminoglycan biosynthesis - heparan sulfate / heparin*	*0.040011*	*5*	*3*
73	**Type II diabetes mellitus**	**0.040011**	**9**	**5**
74	*ABC transporters*	*0.041383*	*8*	*7*

nance, and the vital function of muscles (51, 55). Fibrosis plays a negative role in the potential treatment of DMD because it alters muscle function, reduces the amount of target muscle available for therapy and repair, and considerably reduces the ability of proliferation and differentiation of implanted cells (56, 57). It has been shown that dysregulated and/or disordered ECM proteins also contribute to disease progression in myopathies other than DMD (58, 59). A better understanding of the mechanism that causes muscle fibrosis is important for improving muscle repair and restoring muscle function, which could lead to a potential treatment for DMD. In the present study, we uncovered let-7e-5p-controlled regulation of ECM proteins and demonstrated that dysregulation of let-7e-5p in *mdm* mouse could trigger muscle fibrosis. More precisely, we identified the ECM genes *Col1a1*, *Col1a2*, *Col3a1*, *Col24a1*, *Col27a1*, *Itga1*, *Itga4*, *Scd1*, and *Thbs1* as targets of let-7e-5p. The *in vitro* inhibition of let-7e-5p by its antagomir in pMB^{WT} reversed the stretch-induced suppression of ECM gene expression. In contrast, overexpression of let-7e-5p in pMB^{mdm} revoked the stretch-induced up-regulation of ECM gene expressions. These data confirmed *Col1a1*, *Col1a2*, *Col3a1*, *Col24a1*, *Col27a1*, *Itga1*, *Itga4*, *Scd1*, and *Thbs1* as target genes of mechanomiR-let-7e-5p and support our hypothesis that dys-

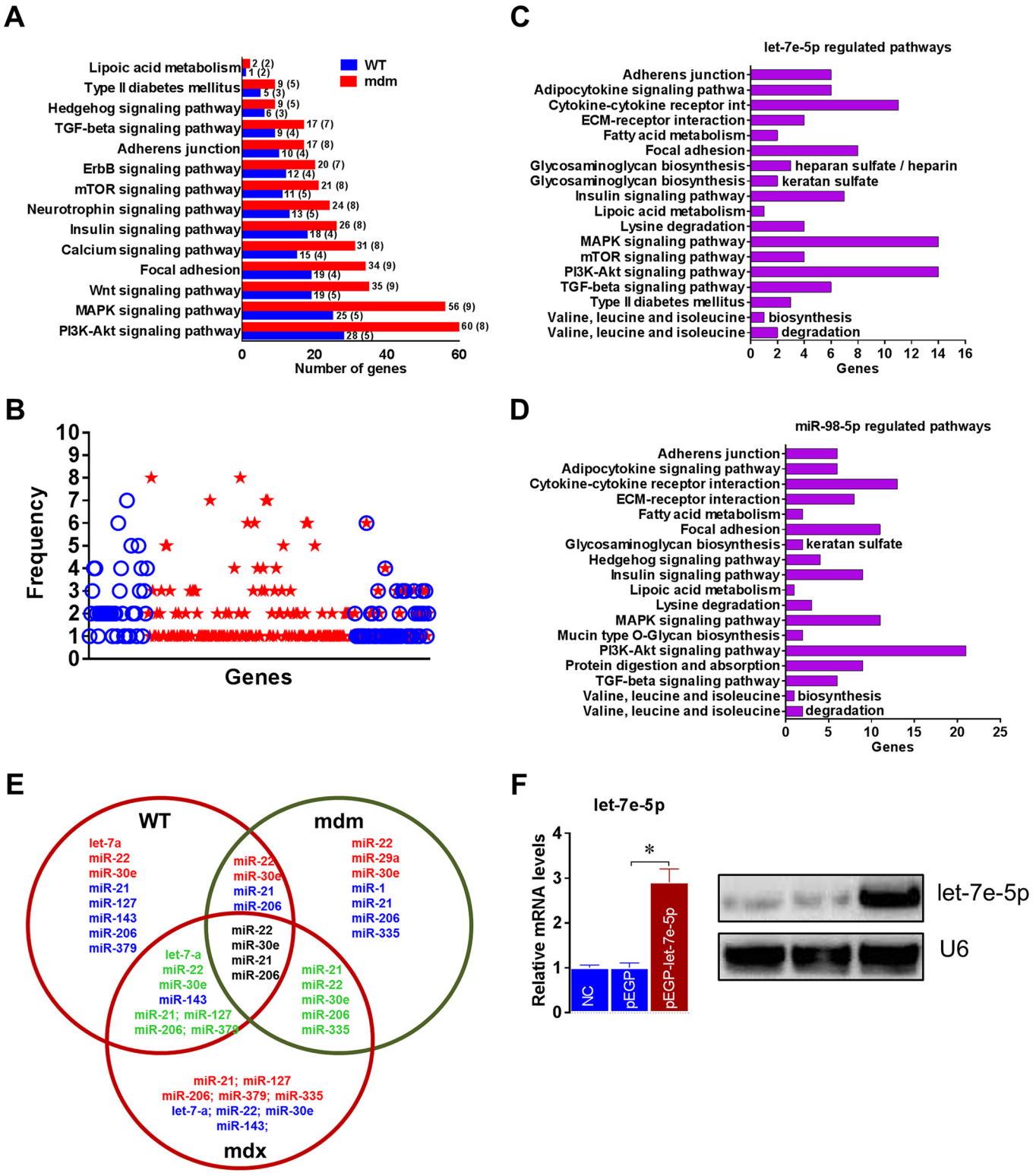

FIGURE 6. **MechanomiR-regulated biological pathways in WT and *mdm* mice.** *A*, mechanomiR-regulated skeletal muscle-specific pathways in both WT and *mdm* mice. *B*, number of genes involved in each pathway (from *A*) in WT (*blue*) or *mdm* (*red*) mice or in both phenotypes. *C* and *D*, let-7e- and miR-98-regulated pathways. *E*, Venn diagram showing a comparison among the differentially regulated mechanomiRs of WT, *mdm*, and *mdx* mice. *F*, pMB^{wt} were stably transfected with either a pEGP empty vector or a pEGP-let-7e-5p vector. Total RNA was isolated after 24 h of transfection and used in real-time PCR and ribonuclease protection assay to measure let-7e-5p levels. U6 was used as a loading control. *Gel pictures* are representative of four independent experiments. Each *bar* represents mean ± S.E. ($n = 4$). *, $p < 0.05$.

regulation of let-7e-5p may contribute to the development of fibrosis in diaphragm muscle from *mdm* mouse. In agreement with these results, we have shown previously that diaphragm muscles from 2-week-old *mdm* mice exhibit moderate fibrosis when compared with severe fibrosis in diaphragm from 6-week-old *mdm* mouse (13). Other investiga-

TABLE 12
Biological pathways regulated by let-7e-5p
Italics indicate skeletal muscle-specific pathways.

No	KEGG pathway	p-value	#genes
1	Transcriptional misregulation in cancer	4.46E-08	14
2	*MAPK signaling pathway*	*3.93E-05*	*14*
3	*Fatty acid metabolism*	*0.000208*	*2*
4	*ECM-receptor interaction*	*0.000208*	*4*
5	*Lysine degradation*	*0.000246*	*4*
6	*Adipocytokine signaling pathway*	*0.000246*	*6*
7	*Valine, leucine and isoleucine biosynthesis*	*0.000653*	*1*
8	Hypertrophic cardiomyopathy (HCM)	0.000653	6
9	*Adherens junction*	*0.000958*	*6*
10	Dilated cardiomyopathy	0.001114	6
11	*Cytokine-cytokine receptor interaction*	*0.001564*	*11*
12	*Glycosaminoglycan biosynthesis - keratan sulfate*	*0.002078*	*2*
13	*PI3K-Akt signaling pathway*	*0.002443*	*14*
14	*TGF-beta signaling pathway*	*0.002495*	*6*
15	*Lipoic acid metabolism*	*0.006045*	*1*
16	Axon guidance	0.010725	8
17	*Insulin signaling pathway*	*0.010725*	*7*
18	*Glycosaminoglycan biosynthesis - heparan sulfate / heparin*	*0.012351*	*3*
19	*Valine, leucine and isoleucine degradation*	*0.013031*	*2*
20	Salmonella infection	0.030946	4
21	*mTOR signaling pathway*	*0.036716*	*4*
22	Hepatitis B	0.039176	6
23	*Type II diabetes mellitus*	*0.0409*	*3*
24	*Focal adhesion*	*0.04193*	*8*

tors have shown that when compared with hindlimb muscle, diaphragm muscle from *mdx* mouse exhibits a high grade fibrosis (47) that recapitulates clinical signs of human DMD (60). In DMD patients, endomysial fibrosis is the only myopathologic parameter that significantly correlates with poor motor outcome at the age of 10 years and at the time of ambulation loss (61). Overall, we uncovered a mechanomiR-mediated regulation of fibrosis in dystrophic skeletal muscle in which suppression of let-7e-5p contributed to the inhibition of proteins that trigger fibrosis in diaphragm from *mdm* mouse. However, further studies are warranted to explore the role of mechanomiRs other than let-7e-5p in regulating fibrosis in dystrophic skeletal muscles.

TGF-β1 is a multifunctional cytokine that plays major roles in many biological pathways including the initiation of fibrosis (49–51). Enhanced TGF-β1 expression has been shown in humans who suffer from MD (51, 62, 63) and mouse models of MDs (48, 50, 64, 65). In line with these findings, in the present study, we observed elevated levels of TGF-β1 in diaphragm muscle from *mdm* mouse. In general, the binding of TGF-β1 to type II receptors and recruitment of type I receptors (ALK4, ALK5, and ALK7) specifically phosphorylate SMAD2 and SMAD3, which produce a nuclear accumulation of active SMAD complexes with SMAD4 that directly regulate gene transcription in conjunction with transcription factors (66). Besides TGF-β1, in the present study, we also observed an increased phosphorylation of SMAD2 and SMAD3 in diaphragm muscle from *mdm* mouse in response to stretch. In contrast, stretch decreased the phosphorylation of SMAD2 and SMAD3 in diaphragm from WT mouse. These results suggest that the TGF-β1 signaling pathway is mechanosensitive and is dysregulated in diaphragm muscle from *mdm* mouse in response to stretch. In agreement with the present study, a previous study has

TABLE 13
Biological pathways regulated by miR-98-5p
Italics indicate skeletal muscle-specific pathways.

No	KEGG pathway	p-value	#genes	#miRNAs
1	Acute myeloid leukemia	0.019117	4	1
2	*Adherens junction*	*0.004361*	*6*	*1*
3	*Adipocytokine signaling pathway*	*0.001089*	*6*	*1*
4	Amoebiasis	5.74E-07	9	1
5	Axon guidance	0.009927	9	1
6	Basal cell carcinoma	0.037042	4	1
7	*Cytokine-cytokine receptor interaction*	*0.001171*	*13*	*1*
8	*ECM-receptor interaction*	*2.65E-24*	*8*	*1*
9	*Fatty acid metabolism*	*0.001089*	*2*	*1*
10	*Focal adhesion*	*0.002844*	*11*	*1*
11	*Glycosaminoglycan biosynthesis - keratan sulfate*	*0.005871*	*2*	*1*
12	*Hedgehog signaling pathway*	*0.016917*	*4*	*1*
13	*Insulin signaling pathway*	*0.001289*	*9*	*1*
14	*Lipoic acid metabolism*	*0.009927*	*1*	*1*
15	*Lysine degradation*	*0.047383*	*3*	*1*
16	*MAPK signaling pathway*	*0.019117*	*11*	*1*
17	Melanogenesis	*0.033633*	*6*	*1*
18	*Mucin type O-Glycan biosynthesis*	*0.003441*	*2*	*1*
19	Pathways in cancer	0.034962	13	1
20	*PI3K-Akt signaling pathway*	*6.69E-07*	*21*	*1*
21	*Protein digestion and absorption*	*2.37E-06*	*9*	*1*
22	Salmonella infection	*0.009956*	*5*	*1*
23	*TGF-beta signaling pathway*	*0.009956*	*6*	*1*
24	Transcriptional misregulation in cancer	0.000188	12	1
25	*Valine, leucine and isoleucine biosynthesis*	*0.001199*	*1*	*1*
26	*Valine, leucine and isoleucine degradation*	*0.036448*	*2*	*1*

shown that mice in which muscle lacking the dystrophin-associated protein γ-sarcoglycan (Sgcg null) were subjected to a lengthening protocol to produce maximal muscle injury, which then produced a rapid accumulation of nuclear phosphorylated SMAD2/3 (67).

Interestingly, the TGF-β1 receptor antagonist suramin attenuates fibrosis in the diaphragm, tibialis anterior, and biceps brachii muscles (47), suggesting that inhibition of the TGF-β1 signaling pathway may be a useful potential alternative therapy for the treatment of DMD. In the present study, we showed that mechanomiRs from WT and *mdm* mice potentially target the genes that are involved in the TGF-β1 signaling pathway (Fig. 6, *A*, *C*, and *D*). Interestingly, many of the predicted genes in the TGF-β1 signaling pathway are potentially targeted by mechanomiRs including let-7e-5p and miR-98, which were up-regulated in diaphragm from WT mouse. In contrast, the majority of the mechanomiRs that were down-regulated in diaphragm from *mdm* mouse appears to target most of the predicted genes in the TGF-β1 signaling pathway. In addition, the loss of mechanosensitivity to miR-98 in diaphragm from *mdm* mouse, along with the observation that miR-98 potentially targets most of the predicted TGF-β1 signaling pathway genes, provides a rationale that supports the possibility of activation of TGF-β1 pathway in *mdm* mice. Overall, patients with MD and animal models of MD, including the *mdm* mouse model, confirm the integral role of TGF-β1 and SMAD signaling in the progression and severity of muscle disease. Further studies are under way in our laboratory to identify the mechanomiR that targets TGF-β1 signaling and that may be beneficial for treating MD.

The let-7 family miRNAs were one of the first miRNAs identified in *Caenorhabditis elegans* (68) and later were found to be

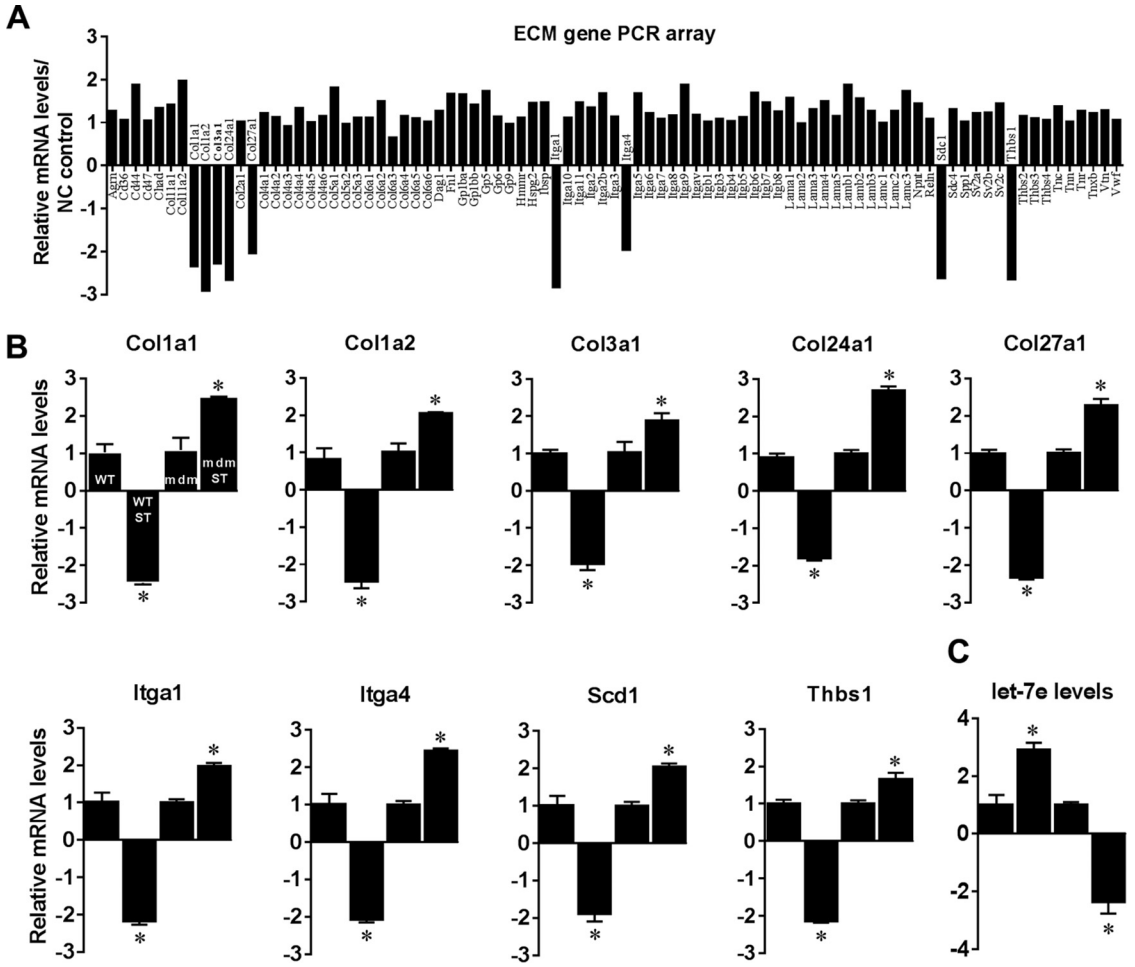

FIGURE 7. **Identification of let-7e-5p target genes.** pMB^{wt} were stably transfected with pEGP or pEGP-let-7e-5p expression construct. *A*, ECM gene mRNA levels in let-7e-5p overexpressed in pMB^{wt} were analyzed 24 h after transfection by real-time PCR array. *B*, expression level of each gene targeted by let-7e-5p was verified in freshly isolated RNA from stretched (*ST*) or unstretched WT and *mdm* mice diaphragms by real-time PCR. *C*, total RNA was isolated from stretched (*ST*) or unstretched pMB^{wt} and pMB^{mdm} and used in real-time PCR to quantify let-7e-5p levels. Each *bar* represents mean ± S.E. ($n = 4$). *, $p < 0.05$ *versus* WT or *mdm*.

conserved across species including mouse and human (69). In the mouse and human, the let-7 family is composed of 10 members (let-7a, -7b, -7c,-7d, -7e, -7f, -7g, and -7i, miR-98, and -202), as recognized by an identical "seed" sequence across those two species (70). Interestingly, all let-7 family members, except miR-202, are mechanomiRs; particularly let-7e-5p (3.27-fold) and miR-98 –5p (2.73-fold) were significantly elevated in response to stretch in WT mice. Although the levels of other let-7 family members (let-7a-5p, -7b-5p, -7c-5p,-7d-5p, and -7f-5p) were between 1.5- and 1.7-fold, their signal intensities in response to stretch were very high (>11,000) in the miRNA array. These results indicate that the let-7 family members are highly regulated mechanomiRs, especially in the diaphragm muscle. Surprisingly, diaphragm muscle from *mdm* mouse displayed down-regulation of the let-7 family members let-7a-5p, -7b-5p, -7c-5p,-7d-5p, -7e-5p, -7f-5p, -7g-5p, and -7i-5p, and especially let-7e-5p, -7f-5p, and -7g-5p, by more than 1.5-fold, indicating dysregulation of the let-7 family of mechanomiRs in dystrophic skeletal muscle. In line with our observation, other investigators have shown that regulation of let-7 is associated with aging and cancer progression. For example, skeletal muscles from elderly people display an elevated levels of let-7b and -7e when compared with that from younger people, and the most highly ranked cellular processes likely to be regulated by let-7b and let-7e miRNAs are associated with cell cycle regulation and cellular growth and proliferation (71). Another study has shown that the primary role of let-7 members is the possession of a conserved function as a tumor suppressor, and therefore they are able to down-regulate the expression of genes associated with cell proliferation, thereby promoting differentiation of human and mouse neuronal stem cells (20). A recent study has identified PABP2 (poly(A)-binding protein) as a genetic interaction partner of the let-7 miRNA (72); the phenotypes associated with human PABP2 mutation in oculopharyngeal MD (a late-onset, progressive disease) seem to affect selectively only muscle cells (73). These studies suggest that the elevated levels of let-7b and let-7e miRNAs in the skeletal muscle of elderly people may contribute to their attenuated skeletal muscle regenerative capacity (74). Taken together, our current findings suggest that the down-regulation of let-7 members, especially let-7e-5p and miR-98-5p in *mdm* mouse, may compromise the ability of these mechanomiRs to increase satellite cell proliferation to improve skeletal muscle regenerative capacity.

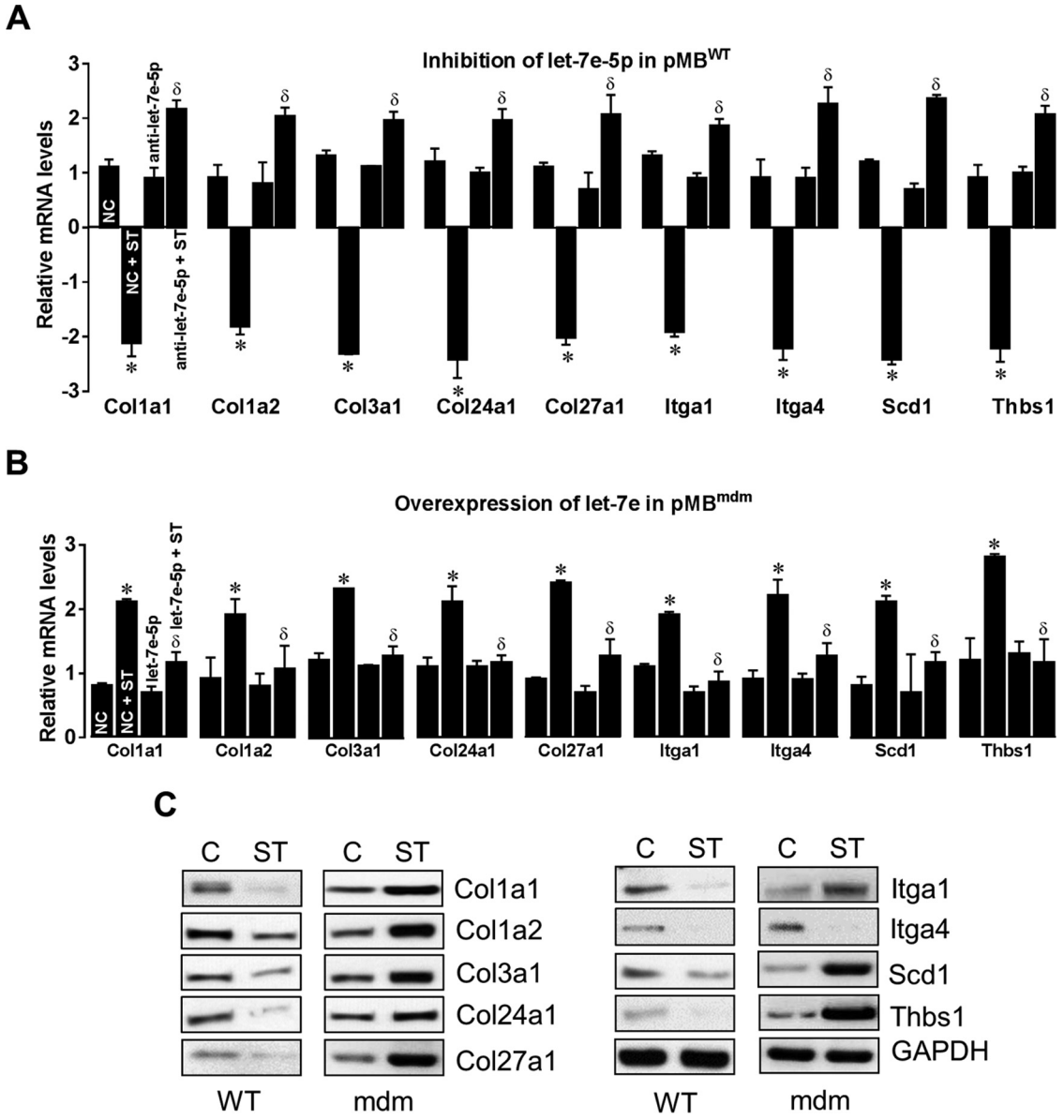

FIGURE 8. ***In vitro* experimental validation of let-7e-5p target genes.** *A*, pMB^{wt} were transfected with let-7e-5p antagomir either in the presence or absence of stretch, and let-7e-5p target gene mRNA levels were determined by real-time PCR. *B*, pMB^{mdm} were transfected with let-7e-5p overexpression construct and subjected to stretch, or no stretch, and let-7e-5p target gene mRNA levels were determined by real-time PCR. *C*, the protein levels of let-7e-5p target genes were determined by Western blot using cell lysate isolated from the unstretched (*C*, control) or stretched (*ST*) diaphragm of WT or *mdm* mouse. GAPDH was used as a loading control. *Gel pictures* are representative of four independent experiments. Each *bar* represents mean ± S.E. ($n = 4$). *, $p < 0.05$, *versus NC* (negative control); δ, $p < 0.05$ *versus NC + ST*.

Furthermore, we have demonstrated previously that mechanical stretch inhibits differentiation and promotes the proliferation of C2C12 myoblasts (6), suggesting that the differentially regulated mechanomiR(s) in diaphragm muscle may regulate myogenesis. To explore this possibility, we transfected pMB^{WT} with the antagomir of let-7e-5p and/or miR-98 and cultured them in differentiation medium with a 1-h stretch for 5 consecutive days. We found that miR-98–5p, but not miR-7e-5p, promoted myoblast differentiation by revoking the inhibitory effect of stretch on differentiation, suggesting a role for mechanomiR-98 in differentiation. In agreement with our study, a previous study has shown that inhibition of miR-98 increases both human (LHCN-M2) and C2C12 myoblast differentiation by directly altering the expression of the transcription factor E2F5, which in turn directly down-regulates the differentiation inhibitors HMOX1 and ID1 (75). Further studies are warranted to confirm the role of other mechanomiRs in myogenesis.

Biaxial loading, in which muscle fibers experience both transverse and longitudinal loads during each respiratory cycle, is the most obvious feature of the mechanical environment of the diaphragm (76). In this study, we applied mechanical stress in either the longitudinal or transverse direction to the muscle fibers, with the magnitude of the mechanical stress along the muscle fibers being essentially the same as that applied in the transverse direction to the muscle fibers. Stress-strain relationship data from our previous studies of the diaphragm clearly demonstrate that muscle compliance is small and extensibility

is reduced in the transverse direction when compared with the longitudinal direction of the muscle fibers (15, 33, 54). In addition, muscle stiffness, a measure of the resistance to mechanical stretch, is greater in the transverse direction of the muscle fibers than in the direction of the fibers (33). In agreement with these studies, data from the present study show that TS differentially regulated a higher number of mechanomiRs (>1.5-fold) compared with LS in the WT mouse (Table 3 and Fig. 1*E*), suggesting that the mechanosensing ability of the WT mouse diaphragm was greater in the transverse direction due to greater transverse muscle stiffness compared with longitudinal stiffness. In contrast, diaphragm muscle from *mdm* mouse showed no difference in the number of mechanomiRs between LS and TS (Table 7 and Fig. 2*E*). However, the number of mechanomiRs that were commonly regulated in response to LS or TS were higher in *mdm* mouse than WT mouse. This suggests that diaphragm muscle from the *mdm* mouse senses greater stiffness in response to longitudinal or transverse directional stretch than diaphragm from age-matched WT mouse as shown previously (13). These data also suggest that the specificity in the mechanosensing ability of the *mdm* mouse diaphragm might be modified due to its dystrophic character. Further studies will be necessary to explore the mechanism by which mechanotransduction is altered in dystrophic skeletal muscle, especially in the diaphragm.

Finally, we performed a comparative analysis between differentially regulated mechanomiRs in *mdm* mouse and previously identified miRNAs (>1.5-fold) in *mdx* mouse skeletal muscle. In the present study, WT and *mdm* mice diaphragms showed up-regulation of the mechanomiRs in let-7a-5p, miR-22–3p, and miR-30e-5p, whereas *mdx* mouse diaphragm showed a down-regulation of these mechanomiRs (Fig. 6*E*). Similarly, the down-regulated mechanomiRs in miR-21a-5p, miR-127–3p, miR-206–3p, miR-335–5p, and miR-379–5p in WT and *mdm* mice were up-regulated in *mdx* mouse skeletal muscle (44).

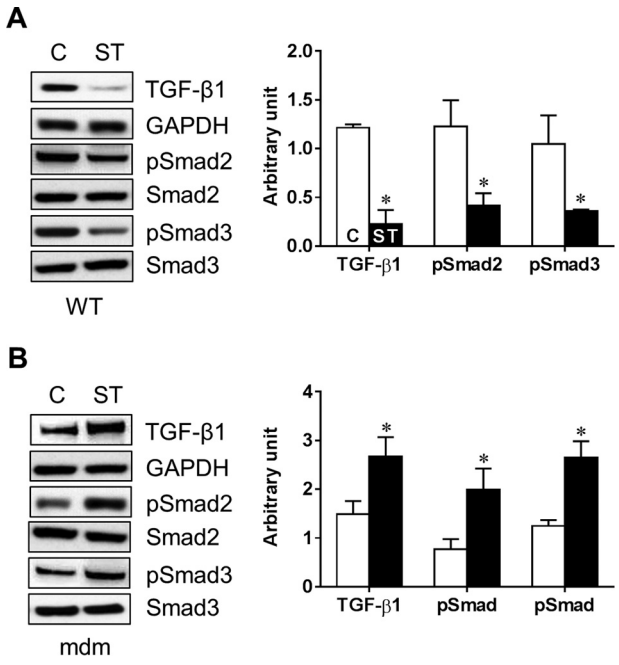

FIGURE 9. **Mechanical stretch alters TGF-β1 signaling pathway.** Diaphragm muscle from WT (*A*) or *mdm* (*B*) mouse were subjected to either LS (*ST*) or left unstretched (*C*, control). Cell lysate was isolated and used in Western blot to measure the expression levels of TGF-β1, SMAD2, and SMAD3 as well as phosphorylated SMAD2 and SMAD3 (pSMAD). GAPDH was used as a loading control. *Gel pictures* are representative of four independent experiments. Each *bar* represents mean ± S.E. ($n = 4$). *, $p < 0.05$ *versus* control.

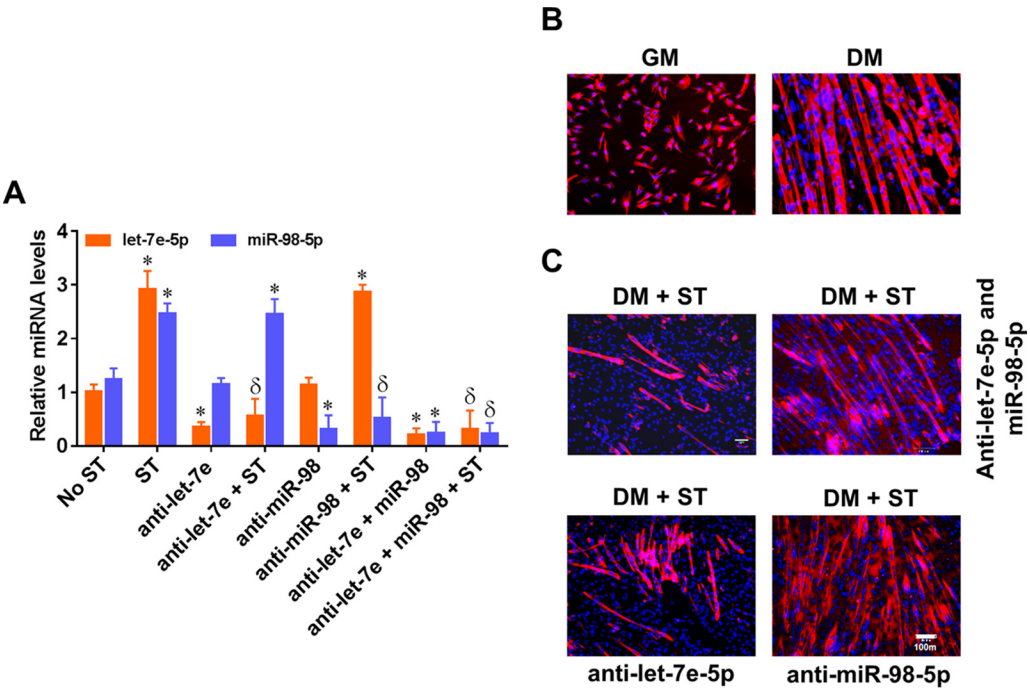

FIGURE 10. **MechanomiR-98–5p regulates myoblast differentiation.** pMB^{wt} were transfected with let-7e-5p antagomir and/or miR-98–5p antagomir. *A*, let-7e-5p and miR-98–5p levels were determined by real-time PCR after a 24-h transfection in either the presence or absence of stretch (*ST*). *B* and *C*, a portion of pMB^{wt} from *A* were cultured in either *GM* or *DM* for 5 days and subjected to stretch (1 h for every 24 h) or no stretch over the 5-day period. *Photomicrographs* are representative of four independent experiments. Each *bar* represents mean ± S.E. ($n = 4$). *, $p < 0.05$ *versus* corresponding unstretched control. δ, $p < 0.05$ *versus* corresponding stretch.

Although *mdx* and *mdm* mice are mouse models of human MDs, the discrepancy in the regulation of miRNAs most likely is due to the stage of severity of the disease. For example, in the present study, we used 2-week-old *mdm* mice in which the histopathological signs in the diaphragm were largely absent when compared with the 6-week-old *mdm* mouse diaphragm (13). The *mdx* mice used by Greco *et al.* (44) were 2 and 14 months old. Therefore, our experiments utilizing 2-week-old *mdm* mice were conducted before onset of the disease, which may explain the discrepancy in the regulation of miRNAs between *mdx* and *mdm* mice. Moreover, the contrasting pathophysiology in skeletal muscles between *mdx* and *mdm* mice is most likely due to the dysfunction of different cytoskeletal proteins (*mdx*, dystrophin; *mdm*, titin), which may contribute to the distinct regulation of miRNAs in these two mouse models.

Author Contributions—J. S. M. designed and wrote the manuscript and performed most experiments. A. H. contributed to bioinformatics and statistical analyses. M. A. L. performed mouse breeding and *ex vivo* experiments. A. M. B. contributed to the design of the study and reviewed and edited the manuscript. All authors reviewed and take full responsibility for the contents of the manuscript. A. M. B. is the guarantor of this work and, as such, had full access to all of the data in the study and takes responsibility for the integrity of the data and the accuracy of the data analysis.

References

1. Hoffman, E. P., Brown, R. H., Jr., and Kunkel, L. M. (1987) Dystrophin: the protein product of the Duchenne muscular dystrophy locus. *Cell* **51,** 919–928
2. Koenig, M., Monaco, A. P., and Kunkel, L. M. (1988) The complete sequence of dystrophin predicts a rod-shaped cytoskeletal protein. *Cell* **53,** 219–228
3. Hackman, P., Vihola, A., Haravuori, H., Marchand, S., Sarparanta, J., De Seze, J., Labeit, S., Witt, C., Peltonen, L., Richard, I., and Udd, B. (2002) Tibial muscular dystrophy is a titinopathy caused by mutations in *TTN*, the gene encoding the giant skeletal-muscle protein titin. *Am. J. Hum. Genet.* **71,** 492–500
4. Kumar, A., Chaudhry, I., Reid, M. B., and Boriek, A. M. (2002) Distinct signaling pathways are activated in response to mechanical stress applied axially and transversely to skeletal muscle fibers. *J. Biol. Chem.* **277,** 46493–46503
5. Kumar, A., and Boriek, A. M. (2003) Mechanical stress activates the nuclear factor-κB pathway in skeletal muscle fibers: a possible role in Duchenne muscular dystrophy. *FASEB J.* **17,** 386–396
6. Kumar, A., Murphy, R., Robinson, P., Wei, L., and Boriek, A. M. (2004) Cyclic mechanical strain inhibits skeletal myogenesis through activation of focal adhesion kinase, Rac-1 GTPase, and NF-κB transcription factor. *FASEB J.* **18,** 1524–1535
7. Mohamed, J. S., Lopez, M. A., Cox, G. A., and Boriek, A. M. (2010) Anisotropic regulation of *Ankrd2* gene expression in skeletal muscle by mechanical stretch. *FASEB J.* **24,** 3330–3340
8. Jaalouk, D. E., and Lammerding, J. (2009) Mechanotransduction gone awry. *Nat. Rev. Mol. Cell Biol.* **10,** 63–73
9. Heydemann, A., and McNally, E. M. (2007) Consequences of disrupting the dystrophin-sarcoglycan complex in cardiac and skeletal myopathy. *Trends Cardiovasc. Med.* **17,** 55–59
10. Kumar, A., Khandelwal, N., Malya, R., Reid, M. B., and Boriek, A. M. (2004) Loss of dystrophin causes aberrant mechanotransduction in skeletal muscle fibers. *FASEB J.* **18,** 102–113
11. Claflin, D. R., and Brooks, S. V. (2008) Direct observation of failing fibers in muscles of dystrophic mice provides mechanistic insight into muscular dystrophy. *Am. J. Physiol. Cell Physiol.* **294,** C651–C658
12. Boriek, A. M., Capetanaki, Y., Hwang, W., Officer, T., Badshah, M., Rodarte, J., and Tidball, J. G. (2001) Desmin integrates the three-dimensional mechanical properties of muscles. *Am. J. Physiol. Cell Physiol.* **280,** C46–C52
13. Lopez, M. A., Pardo, P. S., Cox, G. A., and Boriek, A. M. (2008) Early mechanical dysfunction of the diaphragm in the muscular dystrophy with myositis (Ttnmdm) model. *Am. J. Physiol. Cell Physiol.* **295,** C1092–C1102
14. Mohamed, J. S., Lopez, M. A., Cox, G. A., and Boriek, A. M. (2013) Ankyrin repeat domain protein 2 and inhibitor of DNA binding 3 cooperatively inhibit myoblast differentiation by physical interaction. *J. Biol. Chem.* **288,** 24560–24568
15. Patel, N. D., Jannapureddy, S. R., Hwang, W., Chaudhry, I., and Boriek, A. M. (2003) Altered muscle force and stiffness of skeletal muscles in α-sarcoglycan-deficient mice. *Am. J. Physiol. Cell Physiol.* **284,** C962–C968
16. Lopez, M. A., Mayer, U., Hwang, W., Taylor, T., Hashmi, M. A., Jannapureddy, S. R., and Boriek, A. M. (2005) Force transmission, compliance, and viscoelasticity are altered in the α7-integrin-null mouse diaphragm. *Am. J. Physiol. Cell Physiol.* **288,** C282–C289
17. Bushati, N., and Cohen, S. M. (2007) microRNA functions. *Annu. Rev. Cell Dev. Biol.* **23,** 175–205
18. Sharma, M., Juvvuna, P. K., Kukreti, H., and McFarlane, C. (2014) Mega roles of microRNAs in regulation of skeletal muscle health and disease. *Front. Physiol.* **5,** 239
19. Winbanks, C. E., Ooi, J. Y., Nguyen, S. S., McMullen, J. R., and Bernardo, B. C. (2014) MicroRNAs differentially regulated in cardiac and skeletal muscle in health and disease: potential drug targets? *Clin. Exp. Pharmacol. Physiol.* **41,** 727–737
20. Zacharewicz, E., Lamon, S., and Russell, A. P. (2013) MicroRNAs in skeletal muscle and their regulation with exercise, ageing, and disease. *Front. Physiol.* **4,** 266
21. Callis, T. E., Deng, Z., Chen, J. F., and Wang, D. Z. (2008) Muscling through the microRNA world. *Exp. Biol. Med.* (*Maywood*) **233,** 131–138
22. McCarthy, J. J., Esser, K. A., and Andrade, F. H. (2007) MicroRNA-206 is overexpressed in the diaphragm but not the hindlimb muscle of *mdx* mouse. *Am. J. Physiol. Cell Physiol.* **293,** C451–C457
23. Mohamed, J. S., Lopez, M. A., and Boriek, A. M. (2010) Mechanical stretch up-regulates microRNA-26a and induces human airway smooth muscle hypertrophy by suppressing glycogen synthase kinase-3β. *J. Biol. Chem.* **285,** 29336–29347
24. Guan, Y. J., Yang, X., Wei, L., and Chen, Q. (2011) MiR-365: a mechanosensitive microRNA stimulates chondrocyte differentiation through targeting histone deacetylase 4. *FASEB J.* **25,** 4457–4466
25. Huang, Y., Crawford, M., Higuita-Castro, N., Nana-Sinkam, P., and Ghadiali, S. N. (2012) miR-146a regulates mechanotransduction and pressure-induced inflammation in small airway epithelium. *FASEB J.* **26,** 3351–3364
26. Kobus, K., Kopycinska, J., Kozlowska-Wiechowska, A., Urasinska, E., Kempinska-Podhorodecka, A., Haas, T. L., Milkiewicz, P., and Milkiewicz, M. (2012) Angiogenesis within the duodenum of patients with cirrhosis is modulated by mechanosensitive Kruppel-like factor 2 and microRNA-126. *Liver Int.* **32,** 1222–1232
27. Kumar, S., Kim, C. W., Simmons, R. D., and Jo, H. (2014) Role of flow-sensitive microRNAs in endothelial dysfunction and atherosclerosis: mechanosensitive athero-miRs. *Arterioscler. Thromb. Vasc. Biol.* **34,** 2206–2216
28. Marin, T., Gongol, B., Chen, Z., Woo, B., Subramaniam, S., Chien, S., and Shyy, J. Y. (2013) Mechanosensitive microRNAs-role in endothelial responses to shear stress and redox state. *Free Radic. Biol. Med.* **64,** 61–68
29. Mendias, C. L., Gumucio, J. P., and Lynch, E. B. (2012) Mechanical loading and TGF-β change the expression of multiple miRNAs in tendon fibroblasts. *J. Appl. Physiol.* **113,** 56–62
30. Son, D. J., Kumar, S., Takabe, W., Kim, C. W., Ni, C. W., Alberts-Grill, N., Jang, I. H., Kim, S., Kim, W., Won Kang, S., Baker, A. H., Woong Seo, J., Ferrara, K. W., and Jo, H. (2013) The atypical mechanosensitive microRNA-712 derived from pre-ribosomal RNA induces endothelial inflammation and atherosclerosis. *Nat. Commun.* **4,** 3000

31. Wei, F., Liu, D., Feng, C., Zhang, F., Yang, S., Hu, Y., Ding, G., and Wang, S. (2015) microRNA-21 Mediates stretch-induced osteogenic differentiation in human periodontal ligament stem cells. *Stem Cells Dev.* **24,** 312–319
32. Mohamed, J. S., Hajira, A., Li, Z., Paulin, D., and Boriek, A. M. (2011) Desmin regulates airway smooth muscle hypertrophy through early growth-responsive protein-1 and microRNA-26a. *J. Biol. Chem.* **286,** 43394–43404
33. Boriek, A. M., Zhu, D., Zeller, M., and Rodarte, J. R. (2001) Inferences on force transmission from muscle fiber architecture of the canine diaphragm. *Am. J. Physiol. Regul. Integr. Comp. Physiol.* **280,** R156–R165
34. Garvey, S. M., Rajan, C., Lerner, A. P., Frankel, W. N., and Cox, G. A. (2002) The muscular dystrophy with myositis (*mdm*) mouse mutation disrupts a skeletal muscle-specific domain of titin. *Genomics* **79,** 146–149
35. Ono, Y., Shimada, H., Sorimachi, H., Richard, I., Saido, T. C., Beckmann, J. S., Ishiura, S., and Suzuki, K. (1998) Functional defects of a muscle-specific calpain, p94, caused by mutations associated with limb-girdle muscular dystrophy type 2A. *J. Biol. Chem.* **273,** 17073–17078
36. Vlachos, I. S., Kostoulas, N., Vergoulis, T., Georgakilas, G., Reczko, M., Maragkakis, M., Paraskevopoulou, M. D., Prionidis, K., Dalamagas, T., and Hatzigeorgiou, A. G. (2012) DIANA miRPath v.2.0: investigating the combinatorial effect of microRNAs in pathways. *Nucleic Acids Res.* **40,** W498–W504
37. Dweep, H., Sticht, C., Pandey, P., and Gretz, N. (2011) miRWalk-database: prediction of possible miRNA binding sites by "walking" the genes of three genomes. *J. Biomed. Inform.* **44,** 839–847
38. Mohamed, J. S., Hajira, A., Pardo, P. S., and Boriek, A. M. (2014) MicroRNA-149 inhibits PARP-2 and promotes mitochondrial biogenesis via SIRT-1/PGC-1α network in skeletal muscle. *Diabetes* **63,** 1546–1559
39. Doench, J. G., and Sharp, P. A. (2004) Specificity of microRNA target selection in translational repression. *Genes Dev.* **18,** 504–511
40. Alexander, M. S., Kawahara, G., Motohashi, N., Casar, J. C., Eisenberg, I., Myers, J. A., Gasperini, M. J., Estrella, E. A., Kho, A. T., Mitsuhashi, S., Shapiro, F., Kang, P. B., and Kunkel, L. M. (2013) MicroRNA-199a is induced in dystrophic muscle and affects WNT signaling, cell proliferation, and myogenic differentiation. *Cell Death Differ.* **20,** 1194–1208
41. Alexander, M. S., Casar, J. C., Motohashi, N., Myers, J. A., Eisenberg, I., Gonzalez, R. T., Estrella, E. A., Kang, P. B., Kawahara, G., and Kunkel, L. M. (2011) Regulation of DMD pathology by an ankyrin-encoded miRNA. *Skelet. Muscle* **1,** 27
42. Cacchiarelli, D., Incitti, T., Martone, J., Cesana, M., Cazzella, V., Santini, T., Sthandier, O., and Bozzoni, I. (2011) miR-31 modulates dystrophin expression: new implications for Duchenne muscular dystrophy therapy. *EMBO Rep.* **12,** 136–141
43. Eisenberg, I., Eran, A., Nishino, I., Moggio, M., Lamperti, C., Amato, A. A., Lidov, H. G., Kang, P. B., North, K. N., Mitrani-Rosenbaum, S., Flanigan, K. M., Neely, L. A., Whitney, D., Beggs, A. H., Kohane, I. S., and Kunkel, L. M. (2007) Distinctive patterns of microRNA expression in primary muscular disorders. *Proc. Natl. Acad. Sci. U.S.A.* **104,** 17016–17021
44. Greco, S., De Simone, M., Colussi, C., Zaccagnini, G., Fasanaro, P., Pescatori, M., Cardani, R., Perbellini, R., Isaia, E., Sale, P., Meola, G., Capogrossi, M. C., Gaetano, C., and Martelli, F. (2009) Common micro-RNA signature in skeletal muscle damage and regeneration induced by Duchenne muscular dystrophy and acute ischemia. *FASEB J.* **23,** 3335–3346
45. Roberts, T. C., Blomberg, K. E., McClorey, G., El Andaloussi, S., Godfrey, C., Betts, C., Coursindel, T., Gait, M. J., Smith, C. I., and Wood, M. J. (2012) Expression analysis in multiple muscle groups and serum reveals complexity in the microRNA transcriptome of the *mdx* mouse with implications for therapy. *Mol. Ther. Nucleic Acids* **1,** e39
46. Wang, L., Zhou, L., Jiang, P., Lu, L., Chen, X., Lan, H., Guttridge, D. C., Sun, H., and Wang, H. (2012) Loss of miR-29 in myoblasts contributes to dystrophic muscle pathogenesis. *Mol. Ther.* **20,** 1222–1233
47. Taniguti, A. P., Pertille, A., Matsumura, C. Y., Santo Neto, H., and Marques, M. J. (2011) Prevention of muscle fibrosis and myonecrosis in *mdx* mice by suramin, a TGF-β1 blocker. *Muscle Nerve* **43,** 82–87
48. Zhou, L., Porter, J. D., Cheng, G., Gong, B., Hatala, D. A., Merriam, A. P., Zhou, X., Rafael, J. A., and Kaminski, H. J. (2006) Temporal and spatial mRNA expression patterns of TGF-β1, 2, 3 and TβRI, II, III in skeletal muscles of *mdx* mice. *Neuromuscul. Disord.* **16,** 32–38
49. Vidal, B., Serrano, A. L., Tjwa, M., Suelves, M., Ardite, E., De Mori, R., Baeza-Raja, B., Martínez de Lagrán, M., Lafuste, P., Ruiz-Bonilla, V., Jardí, M., Gherardi, R., Christov, C., Dierssen, M., Carmeliet, P., Degen, J. L., Dewerchin, M., and Muñoz-Cánoves, P. (2008) Fibrinogen drives dystrophic muscle fibrosis via a TGFβ/alternative macrophage activation pathway. *Genes Dev.* **22,** 1747–1752
50. Hartel, J. V., Granchelli, J. A., Hudecki, M. S., Pollina, C. M., and Gosselin, L. E. (2001) Impact of prednisone on TGF-β1 and collagen in diaphragm muscle from *mdx* mice. *Muscle Nerve* **24,** 428–432
51. Bernasconi, P., Torchiana, E., Confalonieri, P., Brugnoni, R., Barresi, R., Mora, M., Cornelio, F., Morandi, L., and Mantegazza, R. (1995) Expression of transforming growth factor-β1 in dystrophic patient muscles correlates with fibrosis: pathogenetic role of a fibrogenic cytokine. *J. Clin. Invest.* **96,** 1137–1144
52. Cohn, R. D., van Erp, C., Habashi, J. P., Soleimani, A. A., Klein, E. C., Lisi, M. T., Gamradt, M., ap Rhys, C. M., Holm, T. M., Loeys, B. L., Ramirez, F., Judge, D. P., Ward, C. W., and Dietz, H. C. (2007) Angiotensin II type 1 receptor blockade attenuates TGF-β-induced failure of muscle regeneration in multiple myopathic states. *Nat. Med.* **13,** 204–210
53. Mehra, A., and Wrana, J. L. (2002) TGF-beta and the Smad signal transduction pathway. *Biochem. Cell Biol.* **80,** 605–622
54. Kumar, S., Kim, C. W., Simmons, R. D., and Jo, H. (2014) Role of flow-sensitive microRNAs in endothelial dysfunction and atherosclerosis: mechanosensitive athero-miRs. *Arterioscler. Thromb. Vasc. Biol.* **34,** 2206–2216
55. Mann, C. J., Perdiguero, E., Kharraz, Y., Aguilar, S., Pessina, P., Serrano, A. L., and Muñoz-Cánoves, P. (2011) Aberrant repair and fibrosis development in skeletal muscle. *Skelet. Muscle* **1,** 21
56. Goyenvalle, A., Seto, J. T., Davies, K. E., and Chamberlain, J. (2011) Therapeutic approaches to muscular dystrophy. *Hum. Mol. Genet.* **20,** R69–R78
57. Davies, K. E., and Grounds, M. D. (2007) Modified patient stem cells as prelude to autologous treatment of muscular dystrophy. *Cell Stem Cell* **1,** 595–596
58. MacDonald, E. M., and Cohn, R. D. (2012) TGFβ signaling: its role in fibrosis formation and myopathies. *Curr. Opin. Rheumatol.* **24,** 628–634
59. Schessl, J., Zou, Y., and Bönnemann, C. G. (2006) Congenital muscular dystrophies and the extracellular matrix. *Semin. Pediatr. Neurol.* **13,** 80–89
60. Stedman, H. H., Sweeney, H. L., Shrager, J. B., Maguire, H. C., Panettieri, R. A., Petrof, B., Narusawa, M., Leferovich, J. M., Sladky, J. T., and Kelly, A. M. (1991) The *mdx* mouse diaphragm reproduces the degenerative changes of Duchenne muscular dystrophy. *Nature* **352,** 536–539
61. Desguerre, I., Mayer, M., Leturcq, F., Barbet, J. P., Gherardi, R. K., and Christov, C. (2009) Endomysial fibrosis in Duchenne muscular dystrophy: a marker of poor outcome associated with macrophage alternative activation. *J. Neuropathol. Exp. Neurol.* **68,** 762–773
62. Yamazaki, M., Minota, S., Sakurai, H., Miyazono, K., Yamada, A., Kanazawa, I., and Kawai, M. (1994) Expression of transforming growth factor-β1 and its relation to endomysial fibrosis in progressive muscular dystrophy. *Am. J. Pathol.* **144,** 221–226
63. Sun, G., Haginoya, K., Wu, Y., Chiba, Y., Nakanishi, T., Onuma, A., Sato, Y., Takigawa, M., Iinuma, K., and Tsuchiya, S. (2008) Connective tissue growth factor is overexpressed in muscles of human muscular dystrophy. *J. Neurol. Sci.* **267,** 48–56
64. Gosselin, L. E., Williams, J. E., Deering, M., Brazeau, D., Koury, S., and Martinez, D. A. (2004) Localization and early time course of TGF-β1 mRNA expression in dystrophic muscle. *Muscle Nerve* **30,** 645–653
65. Andreetta, F., Bernasconi, P., Baggi, F., Ferro, P., Oliva, L., Arnoldi, E., Cornelio, F., Mantegazza, R., and Confalonieri, P. (2006) Immunomodulation of TGF-β1 in *mdx* mouse inhibits connective tissue proliferation in diaphragm but increases inflammatory response: implications for antifibrotic therapy. *J. Neuroimmunol.* **175,** 77–86
66. Schmierer, B., and Hill, C. S. (2007) TGF β-SMAD signal transduction: molecular specificity and functional flexibility. *Nat. Rev. Mol. Cell Biol.* **8,** 970–982

67. Goldstein, J. A., Bogdanovich, S., Beiriger, A., Wren, L. M., Rossi, A. E., Gao, Q. Q., Gardner, B. B., Earley, J. U., Molkentin, J. D., and McNally, E. M. (2014) Excess SMAD signaling contributes to heart and muscle dysfunction in muscular dystrophy. *Hum. Mol. Genet.* **23,** 6722–6731
68. Reinhart, B. J., Slack, F. J., Basson, M., Pasquinelli, A. E., Bettinger, J. C., Rougvie, A. E., Horvitz, H. R., and Ruvkun, G. (2000) The 21-nucleotide let-7 RNA regulates developmental timing in *Caenorhabditis elegans*. *Nature* **403,** 901–906
69. Lagos-Quintana, M., Rauhut, R., Meyer, J., Borkhardt, A., and Tuschl, T. (2003) New microRNAs from mouse and human. *RNA* **9,** 175–179
70. Roush, S., and Slack, F. J. (2008) The let-7 family of microRNAs. *Trends Cell Biol.* **18,** 505–516
71. Drummond, M. J., McCarthy, J. J., Sinha, M., Spratt, H. M., Volpi, E., Esser, K. A., and Rasmussen, B. B. (2011) Aging and microRNA expression in human skeletal muscle: a microarray and bioinformatics analysis. *Physiol. Genomics* **43,** 595–603
72. Hurschler, B. A., Harris, D. T., and Grosshans, H. (2011) The type II poly(A)-binding protein PABP-2 genetically interacts with the let-7 miRNA and elicits heterochronic phenotypes in *Caenorhabditis elegans*. *Nucleic Acids Res.* **39,** 5647–5657
73. Brais, B., Bouchard, J. P., Xie, Y. G., Rochefort, D. L., Chrétien, N., Tomé, F. M., Lafrenière, R. G., Rommens, J. M., Uyama, E., Nohira, O., Blumen, S., Korczyn, A. D., Heutink, P., Mathieu, J., Duranceau, A., Codère, F., Fardeau, M., and Rouleau, G. A. (1998) Short GCG expansions in the *PABP2* gene cause oculopharyngeal muscular dystrophy. *Nat. Genet.* **18,** 164–167
74. Carlson, M. E., Suetta, C., Conboy, M. J., Aagaard, P., Mackey, A., Kjaer, M., and Conboy, I. (2009) Molecular aging and rejuvenation of human muscle stem cells. *EMBO Mol. Med.* **1,** 381–391
75. Kropp, J., Degerny, C., Morozova, N., Pontis, J., Harel-Bellan, A., and Polesskaya, A. (2015) miR-98 delays skeletal muscle differentiation by down-regulating E2F5. *Biochem. J.* **466,** 85–93
76. Boriek, A. M., and Rodarte, J. R. (1994) Inferences on passive diaphragm mechanics from gross anatomy. *J. Appl. Physiol.* **77,** 2065–2070